THE EFFECT OF BLADE TORSIONAL ELASTICITY ON HELICOPTER FLIGHT DYNAMICS

A THESIS SUBMITTED TO
THE GRADUATE SCHOOL OF NATURAL AND APPLIED SCIENCES
OF
MIDDLE EAST TECHNICAL UNIVERSITY

BY

EZGİ AKEL

IN PARTIAL FULFILLMENT OF THE REQUIREMENTS
FOR
THE DEGREE OF MASTER OF SCIENCE
IN
AEROSPACE ENGINEERING

OCTOBER 2017

Approval of the thesis:

THE EFFECT OF BLADE TORSIONAL ELASTICITY ON HELICOPTER FLIGHT DYNAMICS

submitted by **EZGİ AKEL** in partial fulfillment of the requirements for the degree of **Master of Science in Aerospace Engineering Department, Middle East Technical University** by,

Prof. Dr. Gülbin Dural Ünver _____
Director, Graduate School of **Natural and Applied Sciences**

Prof. Dr. Ozan Tekinalp _____
Head of Department, **Aerospace Engineering**

Prof. Dr.Altan Kayran _____
Supervisor, **Aerospace Engineering Dept., METU**

Examining Committee Members:

Prof. Dr. Ozan Tekinalp
Aerospace Engineering Dept., METU _____

Prof. Dr. Altan Kayran
Aerospace Engineering Dept., METU _____

Assoc. Prof. Dr. Ali Türker Kutay
Aerospace Engineering Dept., METU _____

Assoc. Prof. Dr. İlkay Yavrucuk
Aerospace Engineering Dept., METU _____

Prof. Dr. Nafiz Alemdaroğlu
Pilot Training Dept., Atılım University _____

Date: _____

I hereby declare that all information in this document has been obtained and presented in accordance with academic rules and ethical conduct. I also declare that, as required by these rules and conduct, I have fully cited and referenced all material and results that are not original to this work.

Name, Last name: Ezgi AKEL

Signature:

ABSTRACT

THE EFFECT OF BLADE TORSIONAL ELASTICITY ON HELICOPTER FLIGHT DYNAMICS

Akel, Ezgi
M.S., Department of Aerospace Engineering
Supervisor: Prof. Dr. Altan Kayran

October 2017, 113 Pages

Helicopter design and test stages require more complex and high fidelity flight dynamic models to aid the design process of the helicopters. In the common approach, rigid rotor blades models are used in the flight dynamics models and since this is a fast modeling method. However, increased flexibility of the rotor blades necessitates the use of elastic blade models to have more accurate prediction of the rotor loads and the control angles. Elasticity brings extra fidelity to the flight dynamics model which is extensively used in design stage of a helicopter.

In this study, an in house helicopter flight dynamics code (TOROS) which is in Matlab/Simulink Environment and developed by TUSAS Helicopter department is used as the analysis tool. This tool includes a trim model and a six degree of freedom helicopter model with blades modeled rigidly modeled in flap, lag and torsional direction. The mathematical model of a helicopter generated in in house tool is first validated with the commercial FLIGHTLAB model. In the next stage, elastic blade model is integrated to TOROS. In this study, in the elastic blade model flexibility is added only to the torsional degree of freedom. The added torsional flexibility of the blade accounts for change in the aerodynamic and inertial forces with respect to rigid

blade model, resulting in more accurate prediction of the control angles. Tip deflections of the torsionally elastic blade is compared with the results of the finite element based multibody dynamics code Dymore. A finite element modelling capability is added to the in house flight dynamics model to perform trim in level flight, autorotation and transient analyses utilizing both rigid and torsionally elastic blade models. Static longitudinal stability analyses of the helicopter are conducted with rigid and elastic blade models to investigate the effect of elastic blade in the torsional direction on the flight mechanics trim analyses and stability. The result of the study is elastic blades in torsional direction has a direct effect on pitch angle of the blades and hence on collective control. The static stability of the system is also affected in a negative way when the blades are elastic in torsion. Elastic effects should be considered during design process.

Keywords: Elastik Blade Modelling, Elastik Torsion, Rotor Elastic Blade Model, Flight Mechanics Elastic Blade Model, Finite Element Method,

ÖZ

BURULMA YÖNÜNDE ELASTİK PALİN HELİKOPTER UÇUŞ DİNAMİĞİNE ETKİSİ

Akel, Ezgi
Yüksek Lisans, Havacılık ve Uzay Mühendisliği Bölümü
Tez Yöneticisi: Prof. Dr. Altan Kayran

Ekim 2017, 113 Sayfa

Helikopter tasarımını kolaylaştırmak için tasarım ve test süreci daha kapsamlı ve yüksek çözünürlüklü modeller gerektirir. Rotor paleri uçuş dinamiği modellerinde genellikle hızlı sonuç almak için katı modellenir. Helikopter pallerinin esnek oluşu. esnek modelleme ihtiyacını da beraberinde getirir. Elastik modelleme yük ve kontrol açılarının daha doğru tahmin edilebilmesini sağlar. Elastik etkilerin dahil edilmesi modele ekstra bir uygunluk derecesi katar ve tasarım süreçlerinde kullanılabilir hale getirir.

Bu çalışmada TUSAS helikopter grubu içinde geliştirilmiş özgün bir uçuş dinamiği kodu (TOROS) kullanılmıştır. TOROS içinde bir trim algoritması bulunur ve altı serbestlik dereceli helikopter modeli içerir. Bu modelde palalar çırpma, sürükleme ve burulma yönünde katı modellenmiştir. Eklenen burulma yönündeki elastik pal modeli, katı modelden farklı olarak aerodinamik ve ataletsel yükleri değiştirir ve bu da kontrol açılarının daha doğru hesaplanmasını sağlar. Palin uç kısmındaki elastik etkiden gelen dönme miktarı, sonlu elemanlar methoduna dayanan ve bir çoklu dinamik modelleme kodu olan Dymore ile karşılaştırılmıştır. Sonlu elemanlar methodu ile elastik analiz

yapabilme seçeneği TOROS'a eklenmiştir. Bu seçenek ile düz uçuş, otorotasyon denge koşulu gibi denge koşulları ve tüm zamana bağlı manevra analizleri hem burulma yönünde elastik hem de katı modelle yapılabilir duruma gelmiştir. Statik boylamsal kararlılık, denge koşulu ve manevra analizleri hem katı hem elastik model ile tekrarlanmış, burulma yönünde elastik modellenen pallerin uçuş mekaniği analizlerine etkisi incelenmiştir. Bu çalışmaların sonucunda burulma yönündeki elastik pal modelinin helikopterin yunuslama açısına direk etkisinden dolayı kollektif komutunu değiştirdiği gözlemlenmiştir. Aynı zamanda helikopterin boylamsal statik kararlılığı da kullanılan elastik model ile birlikte negatif yönde etkilenmiştir. Bu nedenle elastik etkilerin tasarım sürecinde göz önünde bulundurulması gerekmektedir.

Anahtar kelimeler: Elastik Pal Modelleme, Elastik Burulma, Helikopter Elastik Pal Modeli, Uçuş Mekaniği Elastik Pal Modeli, Sonlu Elemanlar Methodu,

to my family

ACKNOWLEDGEMENTS

I would like to express my gratitude and thanks to my supervisor Prof. Dr. Altan Kayran who guided me throughout this work and gave his time and assistance. I am grateful to my colleague Volkan Kargın who guided me through the subject selection of my thesis and supported me throughout this work and also my professional life in flight mechanics. I would like to thank my professor Assoc. Prof. Dr. Ali Türker Kutay for his valuable help and understanding through my thesis period. I would like to thank my professor Assoc. Prof. Dr. İlkay Yavrucuk who inspires me to study on rotorcraft flight dynamics at the very beginning of my aerospace career.

I would like to thank TAI Helicopter Group Flight Mechanics team for their contributions to the development of this simulation code. I am grateful to Muhammed Emre Bilen for his support on generation of Dymore results and the finite element theory basics. Moreover I would like to express my gratitude to Özge Kapulu and Ayşe İlden Ak who always encourage me to complete this study with their valuable advices. I would like to thank all my friends and flight mechanics team for their support throughout this study.

Finally, I would like to thank my parents, my sister and my puppy Köpük for their endless love and for their valuable guidance through my entire life.

TABLE OF CONTENTS

ABSTRACT v

ÖZ vii

ACKNOWLEDGEMENTS x

TABLE OF CONTENTS xi

LIST OF TABLES xiii

LIST OF FIGURES xiv

LIST OF DEFINITIONS AND ABBREVIATIONS xviii

CHAPTERS

1.INTRODUCTION 1

1.1 Aeroelasticity for Flight Dynamics and Previous Studies 3

1.2 Motivation of the Study 4

1.3 Objective and Scope of the Study 5

2.MATHEMATICAL MODELING 7

2.1 Helicopter Basics 7

2.2 Description of Helicopter Flight Dynamics Code with Rigid Blade Model .. 12

2.2.1 Current Blade and Helicopter Model 15

2.2.2 Blade Dynamics and Rigid Degree of Freedom 17

2.3 Flightlab-TOROS Comparison and a Simulation Example in TOROS 22

2.3.1 Comparisons with Flightlab 25

2.3.2 Simulation Example- Entry to Autorotation Maneuver 32

3.AEROELASTIC BEAM-BLADE MODEL WITH TORSIONAL FLEXIBILITY 37

3.1 Development of the Beam-Blade Model Including Torsional Flexibility 37

3.2 Aerodynamic and Inertial Load Calculation 43

3.2.1 Calculation of the Aerodynamic Loads by the Blade Element Method (BEM) 46

3.2.2 Calculation of Inertial Loads with Finite Element Method..... 55

3.3 Integration of Aerodynamic and Inertial Moments to Aeroelastic Solution .. 60

3.4 Static Solution of Beam Blade and Comparison with Dymore..... 63

4.IMPLEMENTATION OF THE AEROELASTIC BEAM BLADE MODEL INTO FLIGHT DYNAMICS 69

4.1 Trim Analysis 70

4.2 Results of Helicopter Trim and Transient Analyses 72

4.2.1 Level Flight 72

4.2.2 Autorotation 77

4.3 Longitudinal Static Stability..... 81

4.4 Transient Analyses 83

4.4.1 Pull Up Maneuver 84

4.4.2 Autorotation Recovery 91

4.4.3 Jump Take Off from Hover 98

5.CONCLUSION 107

REFERENCES 111

LIST OF TABLES

TABLES

Table 1 TOROS Sign Convention 24

LIST OF FIGURES

FIGURES

Figure 1 Rotor Disk in Forward Flight and Definition of the radial and azimuthal positions 8
Figure 2 Fundamental Blade Motions 8
Figure 3 Tip Path Plane 10
Figure 4 Tilt of the Tip Path Plane in Helicopter Motion 11
Figure 5 Hinges of the Helicopter Blade 12
Figure 6 Current Configuration 16
Figure 7 Blade Axis Configuration 17
Figure 8 Rigid Rotor Blade Flapping Forces 18
Figure 9 Rigid Rotor Blade Lag Forces 19
Figure 10 Rotor Blade Pitching Moments and Forces Generating Pitching Moments 21
Figure 11 Propeller Moment on a Blade Section 21
Figure 12 Inertial Hub Body Reference Frame of Simulation Tool 23
Figure 13 Blade Segment Reference Frame of Simulation Tool 23
Figure 14 Body Reference Frame and Euler Angles and Rates 24
Figure 15 Blade and Mass Sections 25
Figure 16 Comparison of Control Angles of Flightlab and Toros during Forward Flight Trim 27
Figure 17 Comparison of Euler Angles and Power Curves of Flightlab and Toros during Forward Flight Trim 28
Figure 18 Comparison of Flapping Angles of Flightlab and TOROS during Forward Flight Trim 29
Figure 19 Comparison of Shaft Forces of Flightlab and Toros during Forward Flight Trim 30

Figure 20 Comparison of Control Angles of Flightlab and TOROS Elastic Blade during Forward Flight Trim 31
Figure 21 Comparison of Euler Angles of Flightlab and TOROS Elastic Blade during Forward Flight Trim 32
Figure 22 Control inputs of the Autorotation Maneuver 33
Figure 23 Euler angles and Power Curves of the Autorotation Maneuver 34
Figure 24 Flapping Angles of the Autorotation Maneuver 35
Figure 25 Forces of the Autorotation Maneuver 35
Figure 26 Moments of the Autorotation Maneuver 36
Figure 27 : Deflections of an Elastic Beam 38
Figure 28 Distribution of Torsional Deflection Through an Element by the Help of Shape Functions 39
Figure 29 A Simple Three-Element Beam and with Torsional Degrees of Freedom Defined 40
Figure 30 Flowchart of the procedure followed for the load calculation in the flight mechanics model 42
Figure 31 Blade Element and Finite Element Computation Points through Blade 42
Figure 32 Flowchart of the Calculation Process of Aerodynamic Segment and Inertial Segment Loads 45
Figure 33 Blade Geometry Used in Simulation Tool 46
Figure 34 Representation of Different Axes Systems in the Simulation Tool Blade 47
Figure 35 Geometric Angle Representation on an Airfoil 51
Figure 36 Blade Element Section in the Boundary of More than One Finite Element Section 54
Figure 37 Feathering and blade axes 56
Figure 38 Tip Path Plane 63
Figure 39 Non Dimensional Stiffness Distribution of the Blade 64
Figure 40 Non Dimensional Polar Moment of Inertia Distribution of the Blade 64
Figure 41 Non Dimensional Mass Distribution of Blade 65
Figure 42 Comparison of TOROS Hover Elastic Torsional Deflection Through Blade with Dymore 66

Figure 43 Comparison of TOROS 140 Knot Elastic Torsional Deflection Through Blade with Dymore 67
Figure 44 Comparison of Roots of Linearized System in Wind Tunnel Trim..... 71
Figure 45 Comparison of Control Angles for Level Flight Velocity Sweep 73
Figure 46 Comparisons of Euler Angles and Main Rotor and Total Power Curves for Level Flight Velocity Sweep..... 74
Figure 47 Comparison of Flapping Angles for Level Flight Velocity Sweep 75
Figure 48 Comparisons of Shaft Forces for Level Flight Velocity Sweep 76
Figure 49 Comparisons of Shaft Moments for Level Flight Velocity Sweep..... 77
Figure 50 Comparison of Controls for Autorotation Velocity Sweep 78
Figure 51 Comparisons of Euler Angles and Main Rotor and Total Power Curves for Autorotation Velocity Sweep. 79
Figure 52 Comparisons of Flapping angles for Autorotation Velocity Sweep 80
Figure 53 Comparisons of Shaft Forces for Autorotation Velocity Sweep 80
Figure 54 Comparisons of Shaft Moments for Autorotation Velocity Sweep 81
Figure 55 Static Longitudinal Stability Test; Longitudinal Cyclic vs Speed Curve .. 83
Figure 56 : Longitudinal Cyclic Input 84
Figure 57 Comparisons of Control angles in the Pull Up Maneuver 85
Figure 58 Comparisons of Euler angles and Power Curves in the Pull Up Maneuver 86
Figure 59 Comparisons of Indicated Airspeed and Load Factor in the Pull Up Maneuver..... 87
Figure 60 Comparisons of Angular Rates in the Pull Up Maneuver 88
Figure 61 Comparisons of Flapping Angles in the Pull Up Maneuver. 89
Figure 62 Comparisons of Shaft Forces in the Pull Up Maneuver 90
Figure 63 Comparisons of the Shaft Moments in Pull Up Maneuver 90
Figure 64 Comparisons of Control Angles in the Autorotation Recovery Maneuver 91
Figure 65 Comparisons of Euler Angles and Power Curves in the Autorotation Recovery Maneuver 93
Figure 66 Comparisons of Indicated Airspeed and Descent Velocity in the Autorotation Recovery Maneuver 94

Figure 67 Comparisons of Angular Velocities in the Autorotation Recovery Maneuver 95
Figure 68 Comparisons of Flapping Angles in the Autorotation Recovery Maneuver 96
Figure 69 Comparisons of Shaft Forces in the Autorotation Recovery Maneuver.... 97
Figure 70 Comparisons of Shaft Moments in the Autorotation Recovery Maneuver 97
Figure 71 Comparison of Control angles in the Jump Take Off from Hover Maneuver 98
Figure 72 Comparison of Euler Angles and Power Curves in the Jump Take Off from Hover Maneuver..... 99
Figure 73 Comparison of Indicated Airspeed and Load Factor in the Jump Take Off from Hover Maneuver..... 100
Figure 74 Comparison of Angular Rates in the Jump Take Off from Hover Maneuver 101
Figure 75 Comparison of Flapping Angles in the Jump Take Off from Hover Maneuver 102
Figure 76 Comparison of Shaft Forces in the Jump Take Off from Hover Maneuver 103
Figure 77 Comparison of Shaft Moments in the Jump Take Off from Hover Maneuver 103
Figure 78 The Control Angles Comparison of Rigid and Elastic Blade with Different Feathering Axis Locations 105
Figure 79 Different Blade Configurations Effect on Elastic Blade Modelling Results 106

LIST OF DEFINITIONS AND ABBREVIATIONS

Collective($\boldsymbol{\theta_0}$) : Collective is a control which is used to make changes to the pitch angle of the main rotor blades and it results in a simultaneous and equal increase or decrease in pitch angle of all main rotor blades.

KIAS: Indicated Airspeed in knots

Lateral Cyclic($\boldsymbol{\theta_{1c}}$): The left and right cyclic control. It puts in one control input into the rotor system at a time through the swash plate.

Longitudinal Cyclic($\boldsymbol{\theta_{1s}}$): The forward and aft cyclic control. It puts in one control input into the rotor system at a time through the swash plate.

Pedal: It is the collective control of ant- torque rotor, i.e. tail rotor of helicopter.

Swash plate: Mechanism transmitting control inputs to helicopter rotor blades.

$\boldsymbol{\beta_0}$**:** Coning angle, collective flapping angle.

$\boldsymbol{\beta_{1c}}$**:** Longitudinal flapping angle.

$\boldsymbol{\beta_{1s}}$**:** Lateral flapping angle.

ζ: Lead Lag angle

β : Flap angle

$\boldsymbol{\theta}$: Pitch angle

$\boldsymbol{\theta_{elastic}}$: Elastic pitch angle

Ω: Rotational speed of rotor

Ψ : Azimuth angle

$\boldsymbol{F_x}$, $\boldsymbol{F_y}$, $\boldsymbol{F_z}$ **:** Shaft forces in x,y,z direction

$\boldsymbol{M_x}$, $\boldsymbol{M_y}$, $\boldsymbol{M_z}$ **:** Shaft moments in x,y,z direction

$\boldsymbol{N_z}$ **:** Load factor in z direction

CHAPTER 1

INTRODUCTION

There is an increase in interest for more reliable and maneuverable helicopters and this result in a need for more reliable and accurate helicopter flight dynamics models in terms of accurate prediction of hub loads, control angles, helicopter attitudes, hence accurate prediction of real life behavior of an helicopter. In order to understand the physical mechanism behind the helicopter design and predict the response of the aircraft, mathematical models with detailed flight dynamics models are required.

The main and tail rotors are the main contributors to the helicopter dynamic response with the force and the moments they generate. Accurate modeling of the helicopter may be achieved by calculating the aerodynamic and inertia loads generated by the main and the tail rotors correctly and incorporating them in the flight dynamics model. Mathematical models should be fast as well as accurate, because they are used in real time simulators. In simulations, trimmed maneuvers are simulated for users and system is perturbed to reach the desired behavior. Accurate, fast and efficient modeling, in other words, accurate fast and efficient prediction of the rotor dynamics is essential.

The mathematical model developed behaves like a system consisting of sub systems that they define the helicopter and its components. The non-linear mathematical model developed is suitable for simulators, trim analysis, aerodynamic force and moment studies, critical loads and case investigations and maneuver modeling.

In order to reach enough fidelity, models have lots of capability that can be used according to the objective of the analysis. In rotor aerodynamics, blade element method is a model which is frequently used. With the blade element method aerodynamic force and moments may be calculated with acceptable accuracy if the

inflow distribution is known. Tilt in the thrust vector results in a change in force and moments that are transferred to the hub. Therefore, flapping model is essential for an accurate model. In order to capture the dynamic behavior of the blade, tip path plane dynamics is essential. Flexible structure mathematical modelling is important to capture the dynamic behavior.

In the helicopter group of Turkish Aerospace Industry (TAI), a tool including six degree of freedom helicopter mathematical model is developed for flight dynamics analyses and needs. It is a generic tool and helicopter flight mechanics analyses can be performed by entering the parameters of the design. This current developed helicopter flight dynamics modelling tool, TOROS, offer choices to the user to generate either a simple or complex helicopter simulation models. On the aerodynamics side, these choices include blade element method and momentum theory, Pitt Peters or Peter-He inflow models, switches for ground effect or wake distortion. However, in the current state, the blades are rigidly modeled for the purposes of flight mechanics analysis. The main motivation of this study is to develop further understanding to the effect of modeling elastic blades on flight mechanics analyses.

Helicopter rotor blades have high aspect ratios and are highly flexible and therefore the effects of aeroelasticity are larger and therefore more important compared to more rigid structures. The aeroelastic response of rotor blades includes elastic deformation in the flapwise, chordwise, and feathering planes of motion.

In the present study, the effect of torsionally elastic rotor blades on the flight dynamics of the helicopter is investigated. Elastic blade model is developed by using a simple finite element method and integrated to in house flight dynamics tool to enhance its modeling capability. In the elastic blade model, flexibility is added only to the torsional degree of freedom to reduce the complexity and to proceed in a controllable manner in the effort to increase the fidelity of the TOROS flight dynamics tool. The added torsional flexibility of the blade accounts for change in the aerodynamic and inertial forces with respect to rigid blade model, resulting in more accurate prediction of the rotor loads and the control angles.

1.1 Aeroelasticity for Flight Dynamics and Previous Studies

Main rotor in a helicopter is responsible from producing the required lift force and overcome fuselage drag. It also helps to control helicopter in trim or maneuvering flight. In flight dynamics simulation, predicting the required power and thrust is important but estimation of the rotor force and the moments is also a critical point. Therefore, rather than modeling the main rotor like a disk, each blade is individually modeled and more detailed rotor dynamic models including the inflow and the aerodynamic models are required for the accurate calculation of the loads. In most of the applications, rotors with individual rigid blades are rigidly modeled. Several examples are available in literature. One of them is the Genhel model formulated by Howlett [1]. Other simulation programs with individual blade modeling are Curtiss [2], Miller and White [3] and the HELISTAB model by Padfield [4].

Brown and Housten [5] emphasized that real flow effects are important for flight dynamics model whereas other advances in rotor dynamics and aerodynamics cannot be isolated from each other. Flexible rotor blade modelling is an important part of rotor dynamics. In rigid blade modelling, only first modes are considered in flap and lag direction and this is only an estimation of a real blade. Real blade is elastic and all of the modes are deforming under the exerted aerodynamic and inertial loads.

Lewis [6] worked on the effect of flexible blade on the dynamics of UH-60 articulated rotor and used a multibody dynamics formulation to investigate the effect of blade flexibility. It is concluded that for the given rotor, the effect of flexible blade increases with increasing flight speed and its effect is low in hover. Lewis also compared his results with the flight test results.

Sturisky and Schrage [7] stated the importance of blade flexibility in addition to the inflow dynamics. This work is done on the articulated rotor of AH-64 and the results represent that by the help of flexible blade and high order dynamic inflow, there is an increase in the accuracy of the response to off axis control inputs. The off axis responses are the responses on the axes different than the control inputs are given. Such as when a longitudinal input is given to the helicopter and it accelerates in

forward flight, longitudinal responses are the on axis responses whereas lateral responses due to coupling etc. are the off axis responses.

Turnour and Celi [8] have developed a methodology to include the elastic blade that has coupled flap- lag and torsion dynamics in flight mechanics applications. The fuselage and inflow equations of "UM-Genhel" flight dynamics model of Kim, Celi and Tischler [9] and the elastic rotor model of Spence and Celi [10] are coupled and an inflow model of Peters, Boyd [11] and He [12] are integrated in this work. The aim is to investigate the influence of the elastic blade and the frequency response of an articulated rotor on flight dynamics through forward flight sweep. At the end of this study articulated rotor model with the elastic blade and with a higher order finite state inflow modelling, does not help to the prediction of more accurate off axis rotor responses for the particular articulated helicopter configuration considered.

Theodore [13] studied the effects of inflow and blade modelling on the prediction accuracy of Bo 105 helicopter rotor response to control inputs. The model is a non real time model with flap-lag-torsion coupled flexible blade and free wake inflow modeling. Bo 105 rotor is a hingeless rotor and the prediction of off axis response to control inputs accurately is not easy. Theodore ends up with a detailed flight dynamics model which has both free wake inflow model and flexible blade model should be the first step to obtain accurate off axis responses.

According to the study of Piziali [14] that helicopter rotor system design is difficult since estimation of performance, blade stresses, and pitch control angles for the specific flight condition. Hence there is three complex task of rotor design one is the prediction of aerodynamic blade loads, the other one is the dynamic response of rotor blades under external forcing, and last but not the least aeroelastic rotorcraft trim.

1.2 Motivation of the Study

In flight mechanics analysis, fast and accurate prediction of the helicopter dynamic behavior is one of the main targets. In modelling the helicopter rotor, inclusion of the elastic blade model increases the fidelity of the flight mechanics analyses since blades

are actually elastic. Elastic blade models are commonly generated by finite element models of the blades. However solving the model with finite element is time consuming for real time operations and is not convenient for flight mechanics applications. Hence, the main motivation of this study is to add basic elastic effects in a time efficient way and look for the effect of elastic blade on flight mechanics analysis of helicopters.

1.3 Objective and Scope of the Study

In order to increase the fidelity of the in house flight dynamics tool and to capture the dynamic behavior of the blade more accurately, in this study elastic blade model is integrated to the helicopter flight dynamics tool. Since the main objective of integrating the elastic blade model with the flight dynamics tool is to investigate the effect of the elastic blade model on the flight dynamics of the helicopter and not to study the aeroelastic stability of rotor blade, only the torsional degree of freedom of the blade is taken into consideration in the elastic modeling of the blade. Since the torsional deformation of the blade sections induces angle of attack, aerodynamics loads are directly affected in trim and transient conditions from the torsional deformation. On the other hand, blades are very rigid in the lead-lag direction and in the present study the blade is considered to be rigid in the lead-lag direction. However, flapwise elasticity of the blade is important because in unsteady conditions elastic part of the flapwise deflection of the blade also induces angle of attack. In the present study, as a first step blade is made flexible only in the torsional direction and it is aimed to resolve all the issues related to the integration of the elastic blade to the in house helicopter flight dynamics tool which is based on rigid blade model. The main goal of the study is to study the effect of blade flexibility in the torsional direction on the control angles and stability characteristics of the helicopter in trim conditions in hover and forward flight and maneuvers. This way it is aimed to increase the fidelity of the in house flight dynamics tool.

CHAPTER 2

MATHEMATICAL MODELING

This chapter describes the development and validation of the helicopter model that is used as a baseline for flight dynamics analyses. Mathematical modeling is given in detail since it has an essential role in predicting the actual behavior of the helicopter.

In this section, basics of helicopter theory and description of the flight dynamics code with the rigid blade is explained. The main features of the mathematical model included in in hose flight dynamics and simulation tool are presented. Some trim and simulation examples from the in house simulation tool are given for the helicopter model with the rigid blade.

In order to validate the model, the commercial tool Flightlab is used. For this purpose a forward flight sweep comparison with FlightLab is presented to form an idea about the consistency of the flight dynamics models analyzed by the in house code TOROS and the commercial tool FlightLab.

2.1 Helicopter Basics

The most important and effective part of the helicopter is the main rotor and its aerodynamic surfaces, i.e, rotor blades. Rotor blades are the main part of helicopters that generate the required lift and thrust to oppose weight and drag and make it possible for the helicopter to fly by the help of aerodynamic forces.

In flight dynamics models of helicopters rigid and elastic blade models are employed. Elastic modelling of the rotor blades improves the accuracy of flight dynamics simulations. In this respect, understanding the basics of rotor blades is essential. Starting from the physical description, blade radius is denoted by R and rotational

speed by Ω as shown in Figure 1. In the United States, positive sign convention for the direction of the rotor rotation is counterclockwise and right side of the rotor disk is called the advancing side while the left side is called the retreating side. The variables r and ψ are the radial and the azimuthal position of blade as shown in Fig.1.

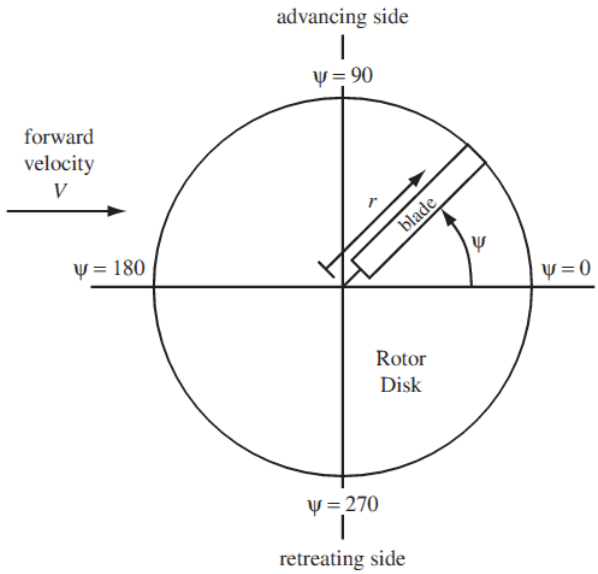

Figure 1 Rotor Disk in Forward Flight and Definition of the radial and azimuthal positions [15]

For constant rotational speed, one can write $\psi = \Omega t$. The rotor blade is normally twisted along its length, θ_{tw}. Rotor blade exhibits three main rigid body rotations; pitching, flapping and lead-lag rotation. Figure 2 shows the fundamental blade motions.

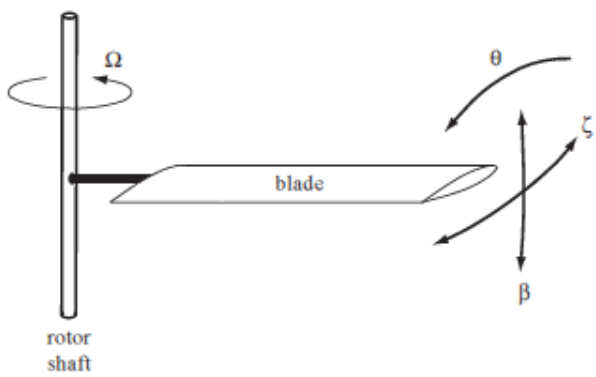

Figure 2 Fundamental Blade Motions [15]

In Fig.2, β is the blade flap angle, it creates a motion out of the rotor disk about the flap hinge. Flapping is positive upwards and negative downwards. δ is the blade lag angle, this degree of freedom creates a motion in the blade disk plane, and lagging is positive when its direction is opposite of the rotor rotation. θ is the blade pitch angle of the feathering motion. Pitching is the rotation of the blade about a hinge, at the feathering (pitch) axis which is parallel to the blade axis. Pitching is positive when leading edge of the blade moves upwards.

Rotor rotates in one direction, clockwise or counterclockwise, and therefore in forward flight; in one side of the rotor the translational velocity and rotational velocity are in the same direction, whereas on the other side, directions of velocities are opposite. Hence there is lack of balance between two sides and this is eliminated by means of rotor flapping. Flapping hinge helps to obtain a symmetrical pressure distribution over the rotor by changing the effective angle of attack due to flapping motion. Dissymmetry of lift is compensated by flapping. Because of the increased airspeed (and corresponding lift increase) on the advancing blade, it flaps upward. Decreasing speed and lift on the retreating blade causes it to flap downward. The induced flow through the flapping motion changes the angle of attack on the blades, and causes the upward flapping advancing blade to produce less lift and downward flapping retreating blade to produce a corresponding lift increase. In the end, lift balances out and it is equal across the disk. It should be noted that as the advancing blade creates more lift, it is allowed to rise and therefore produce less lift. But in doing so, blade's CG moves inward (just like an ice skater tucking his arms in, resulting in an increase in the rotational speed) and rotational speed of the blade increases because the angular momentum of the blade has to be preserved. Hence, linear velocities of the blade sections tend to increase. Therefore, the advancing blade must be allowed to hinge forward to accommodate this speed increase. The reverse happens in the retracting blade.

Tip path plane is the plane that is formed from the union of blade tips after the flapping motion of each blade, as illustrated in Figure 3. Thrust vector can be thought as a vector perpendicular to the tip path plane, so by tilting this plane and changing the direction of the thrust vector helicopter can move back, forward or left and right.

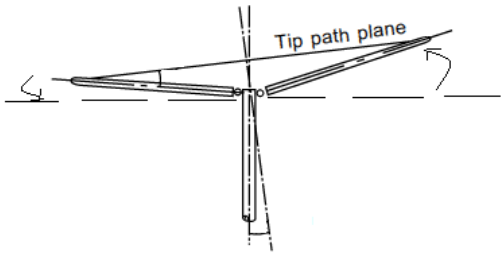

Figure 3 Tip Path Plane [15]

In an helicopter there are certain controls which account for the control of the helicopter during it flight. The collective control changes the pitch angle of all the main rotor blades collectively and independent of their position. Therefore, if a collective input is made, pitch angle of all the blades change equally, and as a result, the helicopter increases or decreases its total lift derived from the rotor. Collective is used to change the attitude and airspeed of the helicopter. The cyclic does the control action by altering the attitude of what is called the rotor disc, i.e., the hypothetical 'disc' the rotors make when they are turning. Actually, what the cyclic is doing is changing the pitch angle of the rotor blades by different amounts, but the net effect is to tilt the rotor disc. The disc then moves in the direction of tilt, and since the rotors are attached to the helicopter fuselage, the body of the helicopter then follows. Moving the cyclic forward causes the rotor disc, and the helicopter, to tilt forward. Moving the cyclic aft has the opposite effect, and moving it sideways causes the helicopter to turn. It can be concluded that collective control changes the magnitude of the thrust vector, cyclic control changes the direction and the magnitude of the thrust vector, as shown in Figure 4.

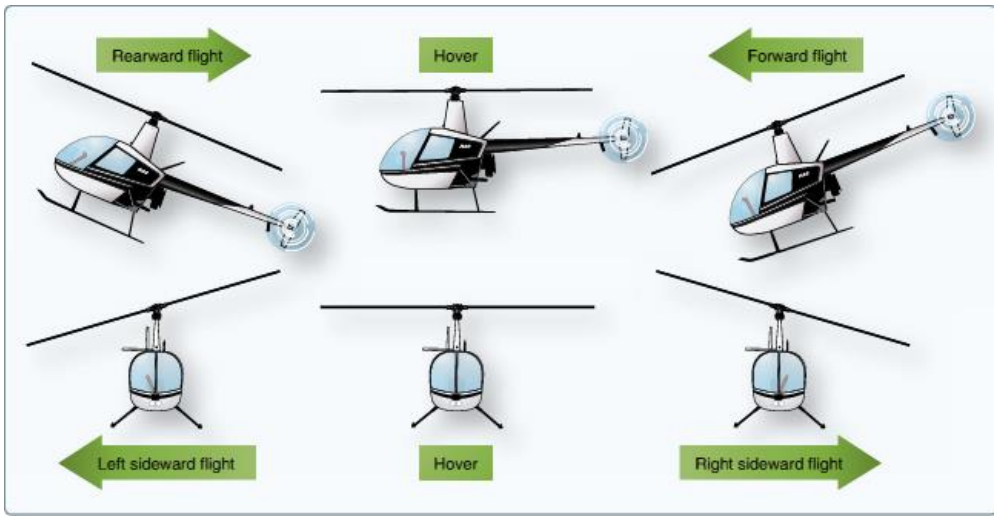

Figure 4 Tilt of the Tip Path Plane in Helicopter Motion [15]

Tail rotor is another significant component of the helicopter. It balances the main rotor torque by the counter moment that is generated with the thrust it produces. Therefore, there is only collective control in the tail rotor. The magnitude of the thrust is generated by the rotor pedal control.

Blade which is free to flap experiences lead-lag motion and to absorb the lead-lag motion lag hinge is needed. Lag hinge allows the release of large Coriolis moments caused by the changing of the CG position of the blade during flapping. Lastly, the blade feathers around a third axis generally parallel to the blade span to allow the change of the pitch angle. Figure 5 shows the hinges in a helicopter blade. The use of blade hinges is an important step in the design period of helicopters since several problems occur by the presence of hinges.

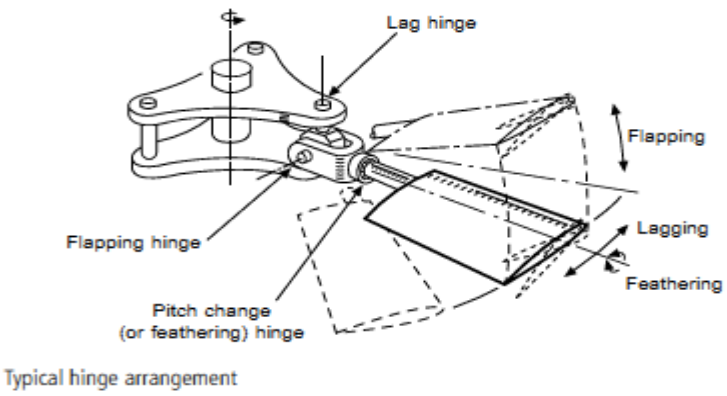

Figure 5 Hinges of the Helicopter Blade [14]

2.2 Description of Helicopter Flight Dynamics Code with Rigid Blade Model

The behavior of helicopter can be modelled as a combination of large number of interacting sub-systems. Among these are the main rotor, the tail rotor, the fuselage, the engines, the flight control system and the empennage with all the forces and moments acting on these elements. A large number of degrees of freedom associated with coupled rotor-body dynamics leads to large number of unknown parameters that have to be estimated [16].

The developed in house flight dynamics model is a multi-dynamic system, acceleration, velocity and position calculated from the six degree of freedom model is transferred to the components. Six degree of freedom model is called 6DOF since the helicopter has both translational and rotational movements about the x-y-z axes. In the 6DOF model, basic equations of motions are solved, and accelerations, velocities and positions are calculated from the forces and the moments of helicopter components and then are transferred to the components.

There should be a component to represent the dynamics of all parts of the helicopter including engine, main and tail rotors, fuselage etc. and these components work in a certain order to provide parameter transfer correctly in the model. In the flow of the simulation, firstly only the integrals of 6 DOF block is run and then environment block,

main rotor, tail rotor, fuselage, empennage, slung load and motor blocks run and lastly 6DOF block itself runs. Velocity and acceleration of the motor are transferred to the main and the tail rotor blocks. Main and tail rotor torque is transferred to the motor model. Motor model is responsible from the power, RPM, torque and fuel flow calculation.

Environmental model deals with air properties and parameters since these change with the altitude. Main rotor module includes the calculation of main rotor inertial, centrifugal and aerodynamic force and moments. Inflow dynamics, blade dynamics, and wake geometry are included in this module. Tail rotor module is responsible from the tail rotor force and moment calculation. The pitching moment contribution of the horizontal tail is important. The lift contribution of horizontal tail to the helicopter center of mass is calculated in the empennage module. Similarly, vertical tail is responsible from the yawing moment and side force contribution to the helicopter center of mass and again modeled in the empennage module. Slung load block is added for the rescue operations when there is a load under helicopter with a sling it directly effects the cg of helicopter and floatation block is added in the need of landing on water which affects the landing gear design directly.

Body accelerations, velocities, control inputs, mass, environment and engine properties of the system are input of the each component and force and moment are the output of each component. Force and moments coming from these components, the main rotor, tail rotor, fuselage, empennage, floatation, slung load and landing gear are summed up and with the environment, mass and engine properties and become the input of the six degree of freedom equations of motion, after these equations of motions are solved, translational velocities, accelerations, Euler angles, angular rates, inertial positions, indicated airspeed, flight path angles and angle of attack and sideslip angles are calculated and transferred again to the components, rotors, engine, fuselage, empennage etc.

Total force and moments from each module are transferred to the center of mass of the total system from the aerodynamic center of each component.

For a successful trim, number of unknowns (floated variables) should be equal to number of constraints which are the targets to be reached or the freezed variables. In other words, there should be a relevant freeze component for each float component for a successful solution. For instance, if the collective is floated, down velocity should be freezed. Iteration is done to reach freezed variables using the Newton Raphson optimization algorithm. After the target is reached, the system is trimmed.

There are two different methods for trim in rotating systems. One of them is to average the rotor forces, moments and states solved at different azimuth angles from 0° to 360° for one blade and transferring these force and moments to the equation of motion equations in 6DOF. The other method is to solve the system for each blade, when the blades are at different azimuths at a single time step, and averaging all inputs, outputs and states. First method is more effective in terms of time and it is preferred in the code.

A trim point or equilibrium point of a dynamic system is where the system is in a steady state. In order to reach trim point, control angles should be set to make system reach that specific condition such as, make the system fly straight and level. In the trim, state derivatives are set to zero, trim starts from an initial point and searches using a trim algorithm, until it finds the nearest trim point. Initial point must be supplied implicit or explicitly.

The mathematical model governing the flight dynamics of a helicopter is a coupled and nonlinear system which can be represented with an ordinary differential equation,

$$\dot{x} = f(x, u, t) \tag{1}$$

where x is the vector of helicopter states which are the parameters to control and $\dot{x}$ is its derivative which should be zero for trim or the equilibrium condition, and u denotes the vector of the inputs and t is the time for simulation which is zero for the trim condition. The derivative of the helicopter states can be initially defined in dynamic trim conditions like maneuvers. The time derivatives of the states, $\dot{x}$, are integrated in time to determine the helicopter states. These new states then become the new inputs of the new (one time step further) simulation.

The aerodynamic properties and coefficients of the current blade model is defined at quarter chord. There is no shear axis offset from feathering axis defined in this model.

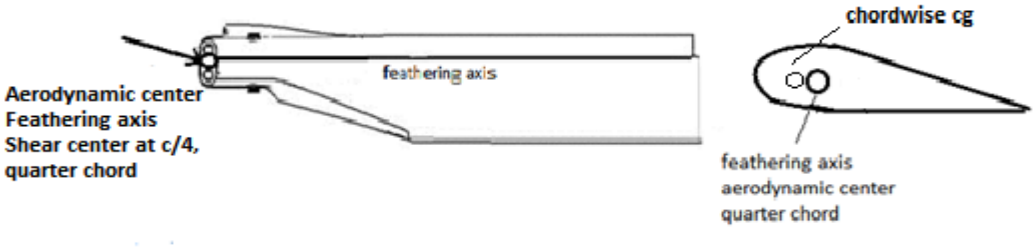

Figure 7 Blade Axis Configuration

For aerodynamic coefficient of the blade table look up is used depending on the local inflow and Mach number. Dynamic inflow models are used like Pitt Peters and Peters-He.

Forces and moments on the main, tail rotor and fuselage acts on their own cg.

2.2.2 Blade Dynamics and Rigid Degree of Freedom

In order to understand the helicopter dynamics, understanding the rigid blade dynamics is important. In this section, rigid body dynamics of flap, lag and torsional degrees of freedom is given with illustrations [15].

The rigid blade model that is used in in house simulation and flight dynamics modelling tool is an articulated model with flap, lead-lag hinges and the pitch link. In the flapping direction, dynamic behavior of the blade is determined by including all the moments acting on the flap hinge and setting the sum of the moments to zero,

$$M_A + M_{CF} + M_{Cor.} + M_I + M_R = 0 \qquad (2)$$

where M_A is the aerodynamic moment, M_{CF} is the centrifugal moment, M_I is the inertial moment, M_{cor} is the Coriolis moment, M_R is the moment created by torsional spring on the flap hinge.

As the moments are written in blade reference frame, positive moments result in an increase in the flap degree of freedom, whereas negative ones result in a decrease in the flap degree of freedom.

The forces acting on the blade resulting rigid flapping are visualized in Figure 8. For a blade with a flap hinge offset (*e*), the out of plane deflection of the blade due to the rigid rotation about the hinge is $z=\beta\eta$ where β is the flapping degree of freedom and the coordinate measured from flap hinge is $\eta=(r-e)$ and *e* is the flap hinge offset.

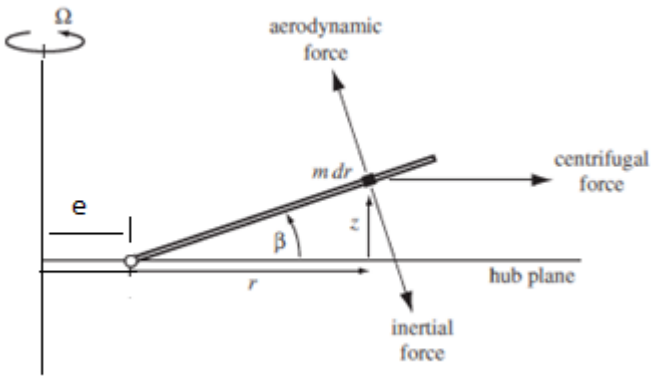

Figure 8 Rigid Rotor Blade Flapping Forces [15]

In Figure 8, *m* is the mass of the section, *dr* is the length of the section, *r* is the distance to the section of interest from the hub, *z* is the vertical displacement due to the flapping motion.

Flapping moments are generated due to: inertial force $m\ddot{z} = m\eta\ddot{\beta}$ with the moment arm *(r-e)*, centrifugal force $m\Omega^2 r$ with the moment arm z=ηβ and aerodynamic force in the z direction of the deflected blade coordinate F_z with the moment arm *(r-e).*

The moment of equilibrium about the flap hinge is given by Eqn.(3)

$$\int_e^R \eta(r-e)mdr\ddot{\beta} + \int_e^R \eta r mdr\Omega^2\beta + K_\beta\beta = \int_e^R (r-e)F_z dr \qquad (3)$$

When Eqn. (3) is rewritten with $I_\beta = \int_e^R \eta^2 mdr$ is defined as the generalized mass moment of inertia with respect to flapping hinge, flapping moment equilibrium equation can be expressed as given in Eqn.(4)

$$I_\beta \ddot{\beta} = M_A - I_\beta \Omega^2 \beta - \Omega^2 e\beta \int_e^R (r-e)\, m dr - K_\beta \beta \quad (4)$$

Moment of torsional spring on flap hinge is given by Eqn. (5),

$$M_R = -K_\beta * \beta \quad (5)$$

In addition to the flapping the motion of blade, in the plane of the disk, blade also undergoes lead-lag motion (ζ) and in articulated rotors there is lag hinge about which the rigid lead-lag motion takes place. The flapping motion generates in plane inertial forces, Coriolis force that results in a coupled flap-lag motion of the blade, hence generally the lag motion requires more complicated analyses.

If the coupling effect is added to flapping equation due to the Coriolis effect, this force will be in the direction opposite to the centrifugal force in Figure 8 and has the magnitude $2\Omega m(r-e)\dot{\zeta}$ with moment arm *(r-e)β*. When the flapping moment of the Coriolis force is integrated from e to R, moment equilibrium equation in the flapping direction can be rewritten as,

$$I_\beta \ddot{\beta} = M_A - I_\beta \Omega^2 \beta - \Omega^2 e\beta\, mr + 2I_\beta \Omega \dot{\zeta} \beta - K_\beta \beta \quad (6)$$

Rigid body lag motion ζ , shown in Figure 9, is positive if its direction is in the opposite direction of the blade rotation. Utilizing the radial coordinate *η=r-e*, for the lead-lag motion, the in-plane deflection can be written as *y=ηζ*. Similar to the flapping hinge, a lag hinge spring constant K_ζ is also included when writing the lead-lag moment equilibrium. The in-plane section forces at the radial location r and their moments arms about the hinge *(r-e)* are shown in Figure 9.

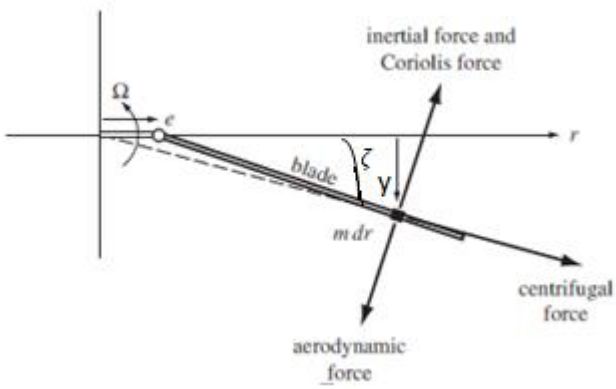

Figure 9 Rigid Rotor Blade Lag Forces [15]

Lagging moments are generated due to: Inertial force $m\ddot{y} = m\eta\ddot{\zeta}$ opposing the lag motion with the moment arm *(r-e)* about the lag hinge, centrifugal force $m\Omega^2 r$ directed radially outward from the center of rotation with the moment arm *y(e/r)=ηζ(e/r)* about the lag hinge, aerodynamic force F_y in the drag direction with the moment arm *(r-e)* and lastly the Coriolis force $2\Omega\dot{z}\acute{z}m = 2\Omega\dot{\beta}\beta(r-e)m$ in the same direction as the inertial force with the moment arm *(r-e).*

It should be noted that if the lag hinge is at the center of rotation, centrifugal force would produce no moment. Coriolis force is the combination of blade rotation and radially inward section velocity $\dot{z}\acute{z}$. The radial velocity is the in-plane component of the flap velocity $\dot{z} = (r-e)\dot{\beta}$ produced when the blade is coned upward $\acute{z} = \frac{dz}{dr} = \beta$.

Equilibrium of these moments about the lag hinge with a spring moment $K_\zeta\zeta$, results in Eqn. (7)

$$\int_e^R \left[\left(m\eta\ddot{\zeta}\right)(r-e) + m\Omega^2 r\left(\frac{e}{r}\eta\zeta\right) + 2\Omega\beta\dot{\beta}(r-e)^2 m\right]dr + K_\zeta\zeta = \int_e^R F_x(r-e)dr \tag{7}$$

Inserting $I_\zeta = \int_e^R \eta^2 m dr$ the lead-lag equation for blade becomes,

$$I_\zeta\ddot{\zeta} = M_A - \Omega^2(r-e)\frac{e}{r}mr - K_\zeta\zeta - I_\zeta 2\Omega\beta\dot{\beta} \tag{8}$$

In the in house model with the rigid blade, the rotor dynamics is also includes the blade pitch degree of freedom. Blade pitch motion is the rigid body rotation about the feathering axis, restrained by the rotor control system. If there is flexibility in the control system, blade pitch motion is a degree of freedom not just a control input. The rotor control system commands a pitch angle θ_{con}, while the actual blade pitch angle is θ. The difference (θ-θ_{con}) is due to control system flexibility and produces a restoring moment about feathering axis given by $K_\theta(\theta - \theta_{con})$ where K_θ is the control system spring constant. Effective moments in the pitch equation are given in Figure 10.

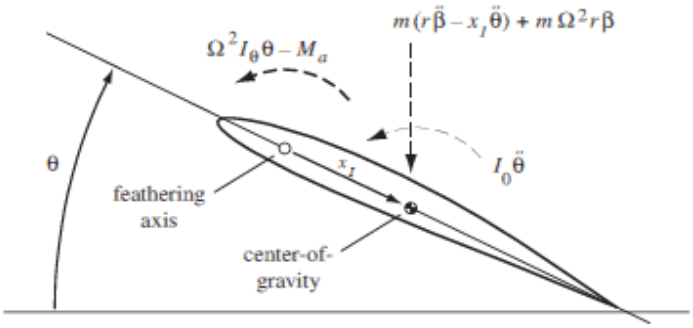

Figure 10 Rotor Blade Pitching Moments and Forces Generating Pitching Moments [15]

The pitch equation of motion is obtained from the equilibrium of moments about the feathering axis. The forces and moments acting on the blade section, which contribute to the pitch equation of motion, can be summarized as:

- Inertial moment $I_0\ddot{\theta}$ about the center of gravity (cg)
- Inertial force $m(r\ddot{\beta} - x_l\ddot{\theta})$ acting on the cg, with moment arm x_l about the feathering axis.
- Propeller moment $I_\theta\Omega^2\theta$ about the feathering axis opposing the pitch motion. Propeller moment is due to centrifugal forces as seen in Figure 11.
- Flapping centrifugal force $m\Omega^2 r\beta$ acting at the cg, with the moment arm x_l about the feathering axis. When the blade flaps up, the component of the centrifugal force normal to the blade and creates centrifugal flapping moment but also since there is an offset between the cg and the feathering axis, it also creates pitch moment.
- Nose up aerodynamic moment M_a about the feathering axis.

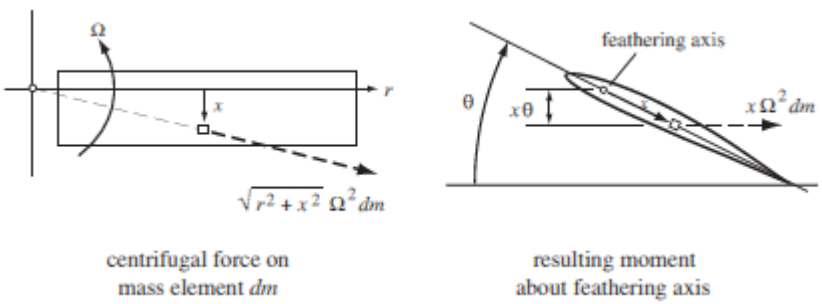

Figure 11 Propeller Moment on a Blade Section [15]

The equilibrium of pitching moments about the feathering axis can be expressed as,

$$\int_0^R \left[I_0\ddot{\theta} - \left(r\ddot{\beta} - x_l\ddot{\theta}\right)x_l m + I_\theta \Omega^2 \theta - m\Omega^2 r\beta x_l\right]dr + K_\theta(\theta - \theta_{con}) = \int_0^R M_a dr \tag{9}$$

where I_0 is the pitching moment of inertia about the cg axis and $I_\theta = I_0 + x^2{}_l m$ is the section moment of inertia about the feathering axis.

2.3 Flightlab-TOROS Comparison and a Simulation Example in TOROS

TOROS is capable to achieve flight dynamics analyses, trims and maneuvers with rigid body dynamics. Trim is an equilibrium point in a given flight condition and maneuvers are achieved by giving control inputs on a trimmed system. By the help of maneuver simulations, one can estimate the possible behavior of the helicopter during the maneuver.

Before giving the results, axis systems and sign conventions of the in house simulation tool is given for further understanding through Figure 12, Figure 13 and Table 1.

In Figure 12 X_B, Y_B, Z_B are the body axes coordinates which moves with the body and translational and rotational velocities, accelerations of the body are defined in this frame. The hub axis is attached to the hub and rotates with hub.

Blade axis, X_b, Y_b, Z_b is attached to blade as in Figure 13, its origin is hinge hence it flaps, lead-lags and feathers with the blade.

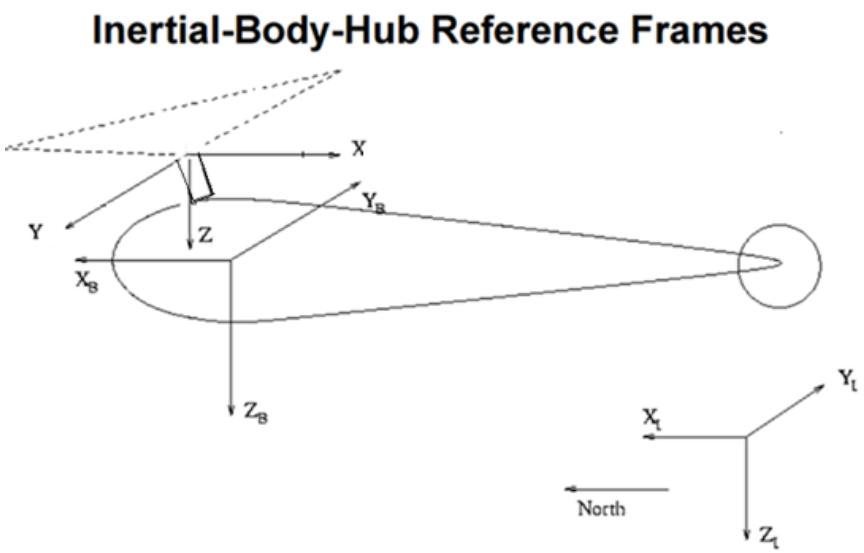

Figure 12 Inertial Hub Body Reference Frame of Simulation Tool

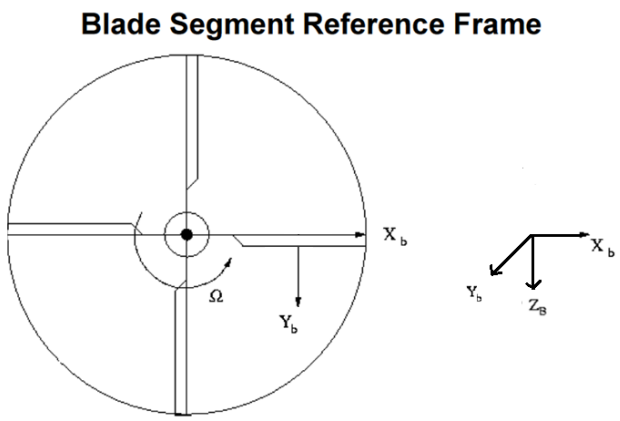

Figure 13 Blade Segment Reference Frame of Simulation Tool

Body angles and angular rates are defined in body axes as shown in Figure 14. For Euler angles positive body pitch is nose up, body roll is starboard and heading is nose right.

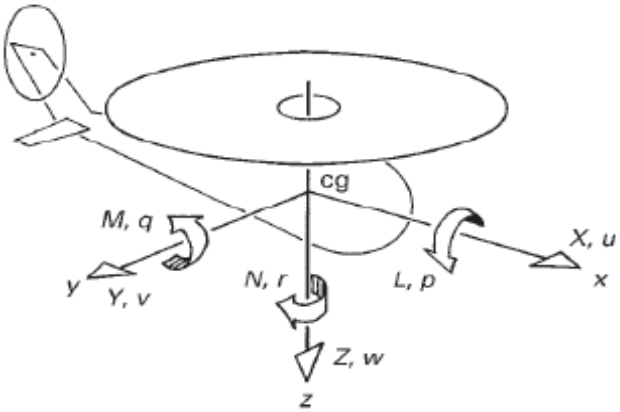

Figure 14 Body Reference Frame and Euler Angles and Rates [15]

Table 1 TOROS Sign Convention

	TOROS	
Theta Collective (θ_0)	Upwards (+)	Downwards(-)
Lon Cyclic (θ_{1s})	Aft (+)	Forward (-)
Lat Cyclic (θ_{1c})	Right (+)	Left (-)
Coning (β_0)	Upward (+)	Downward(-)
Long Flapping (β_{1c})	Backward blade upwards Forward tilt of rotor disk (+)	Backward blade downwards Aft tilt of rotor disk(-)
Lat Flapping (β_{1s})	Right blade upwards Left tilt of rotor disk (+)	Left blade upwards Right tilt of rotor disk(-)
Leadlag (ζ)	Aft(+)	Forward(-)

Figure 15 shows the blade axis whose origin is located at the hinge. In helicopter rotor dynamics, blade axis is needed since blade has rotational motions in each three axis.

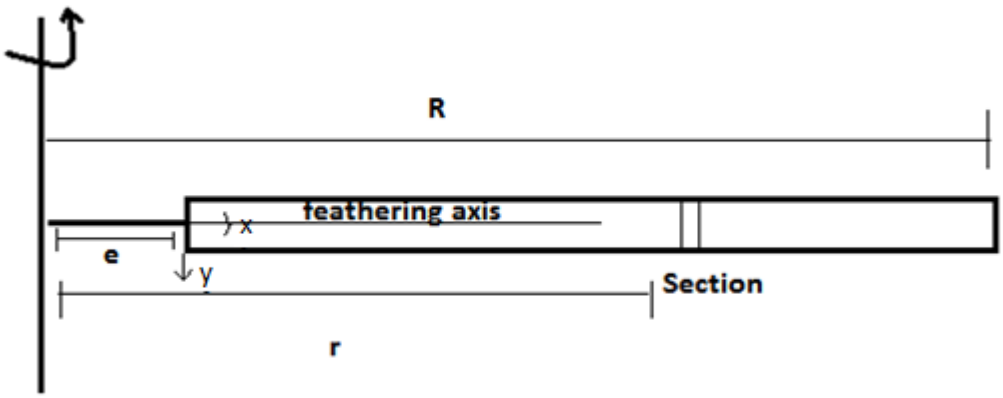

Figure 15 Blade and Mass Sections

In the following section, an indicated airspeed sweep including hover and forward flight trims and an entry to autorotation maneuvers are simulated as an example. A Flightlab comparison are given for the forward flight trim analyses.

2.3.1 Comparisons with Flightlab

One of the validation methods for simulation tools is flight tests which are really expensive and also not an easy process to practice. Another method is validating the flight dynamics tool with a known commercial tool. In this method various results of simulation model are compared with the results of a validated simulation tool. To this end, commercially available tool FlightLab [17] is used for the validation study. The simulation results of the TOROS helicopter model with the rigid blade are compared with FlightLab rigid blade results.

It should be noted that the results given in this section are compatible with in house simulation tool sign convention.

The current helicopter is a 6000 kg civil helicopter with an articulated rotor. Trims for various forward flight speeds including hover are done for the comparison studies between 0 to 120 knots. In the analyses performed, landing gear is retracted, a five

bladed articulated rotor with rigid blade and flap and lag hinge offset is analyzed. Analyses are done at 6000 feet 30℃ atmospheric conditions. It should be noted that both TOROS and Flightlab models are capable of trimming full helicopter model. Main and tail rotors are modelled with blade element where two dimensional aerodynamic panel that produces air loads as non-linear functions of dynamic pressure, angle of attack and Mach number. Blades are rigid. Flap and lag dynamics are included in the analyses. In the main rotor, unsteady potential flow theory of Peters-He is used. Induced inflow distribution at the rotor plane is given as a function of Peters-He inflow radial shape functions. The aerodynamic coefficients are computed using table look ups as functions of angle of attack and Mach number and lift, drag and pitching moment defined in wind frame are computed. The loads in the body frame are computed from lift, drag and pitching moment.

Figure 16 shows the comparison of the control angles calculated by the TOROS and the Flightlab during the hover to 120 knot forward flight trims. Figure 16 shows that control angles calculated by TOROS and Flightlab are close to each other except for the difference in the lateral cyclic behavior, especially during 20-50 knot forward flight speed. This difference is around 0.5 degree which is considered to be small and due to the unavoidable modelling differences between the inflow modelling and the drag modelling of yawed flow in two flight mechanics analysis tools.

The yawed flow drag is the drag caused by the yawed flow on blade which is in the spanwise direction of blade and not exactly equal to the static drag coefficient or the spanwise component of flow. It is between these two values.

speed same as the initial trim speed. Hence lateral speed is held around zero and longitudinal speed is held around 100 knot trim speeds.

From Figure 22 it can be seen that collective is lowered, longitudinal cyclic tries to keep the pitch angle around the trim position to hold the longitudinal speed and lateral cyclic is trying to keep the lateral speed around zero.

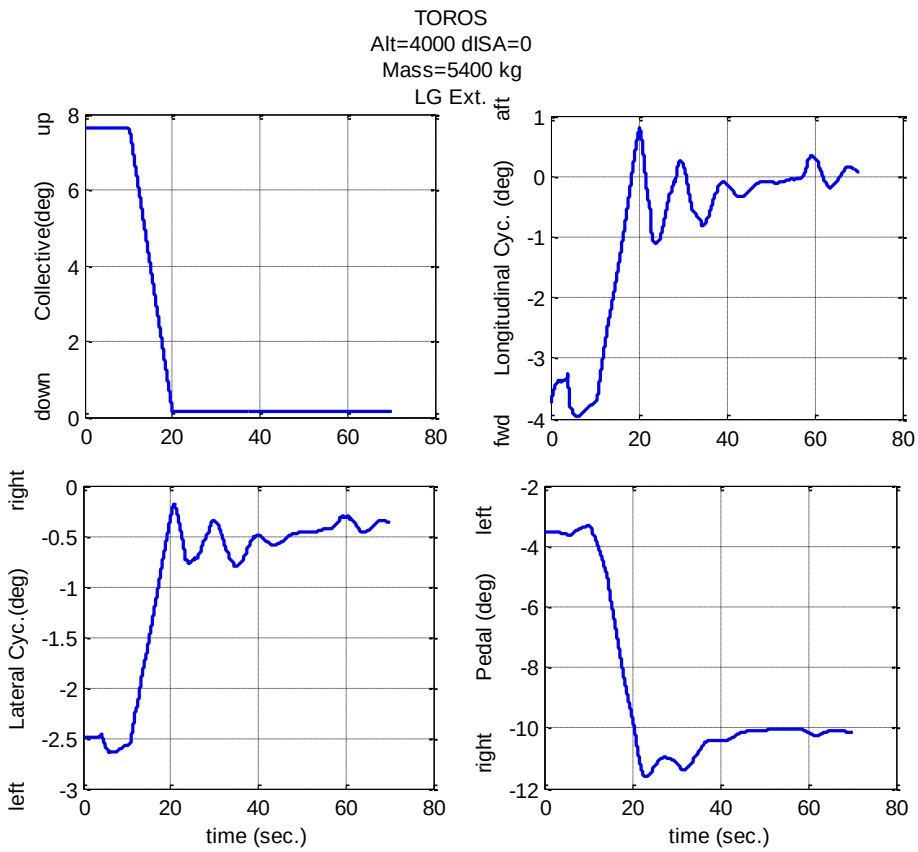

Figure 22 Control inputs of the Autorotation Maneuver

Figure 23 shows the Euler angles and power curves obtained during the simulation of the autorotation maneuver.

From Figure 23, it is seen that the pitch angle is oscillatory around -2°. Since the longitudinal and lateral speed controller is active, controller generates the required pitch and roll angle to keep the lateral and longitudinal speeds constant. The power of the main rotor is zero since autorotation entry is simulated and when the system is in autorotation there is no main rotor power.

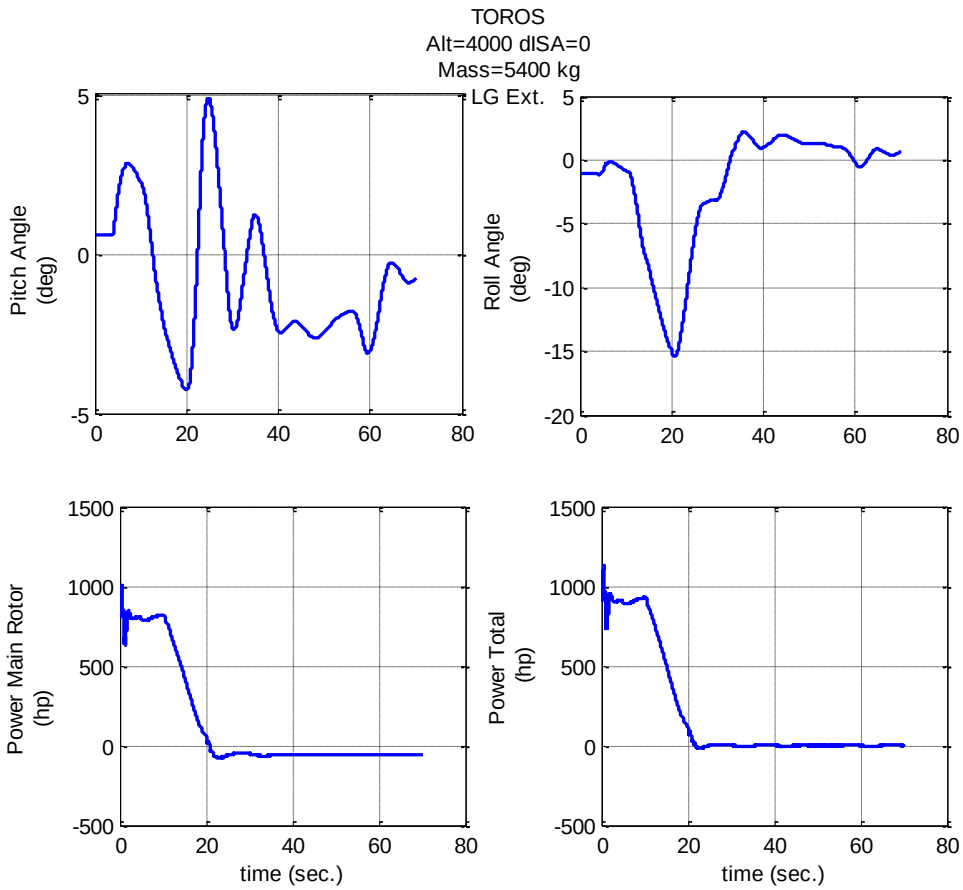

Figure 23 Euler angles and Power Curves of the Autorotation Maneuver

Figure 24 gives the flapping angles of the autorotation maneuver. Figure 25 gives the hub forces calculated during the simulation of the autorotation maneuver. It is seen that the hub force in z direction decreases up to 20 sec. where collective is lowered and system enters autorotation. Since collective decreases moment and force in z direction decreases. M_z moment reaches zero in Figure 26 since system is in autorotation, main rotor power should be zero hence torque is zero. Force F_y reaches zero as lateral cyclic reaches zero.

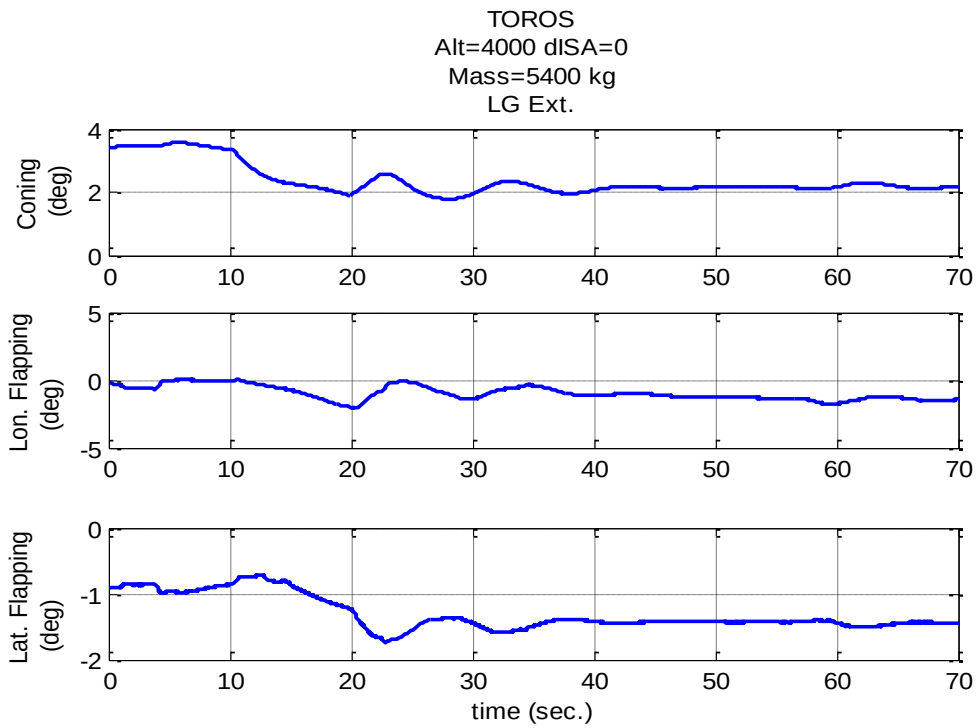

Figure 24 Flapping Angles of the Autorotation Maneuver

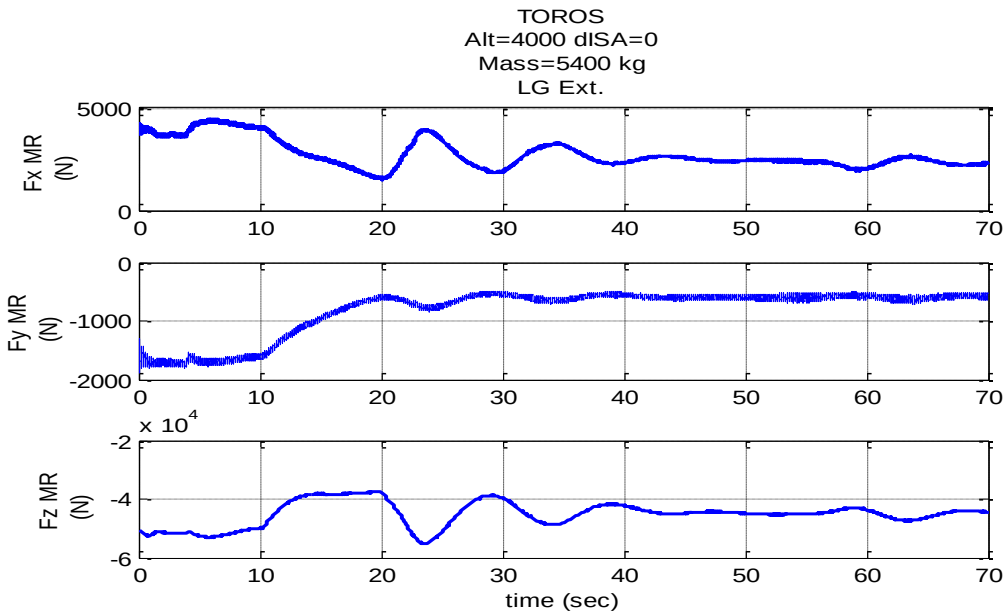

Figure 25 Forces of the Autorotation Maneuver

Total moments are given in Figure 26, moment in y direction is positive which generates a nose up moment. M_x moment is positive and generates a right lateral moment.

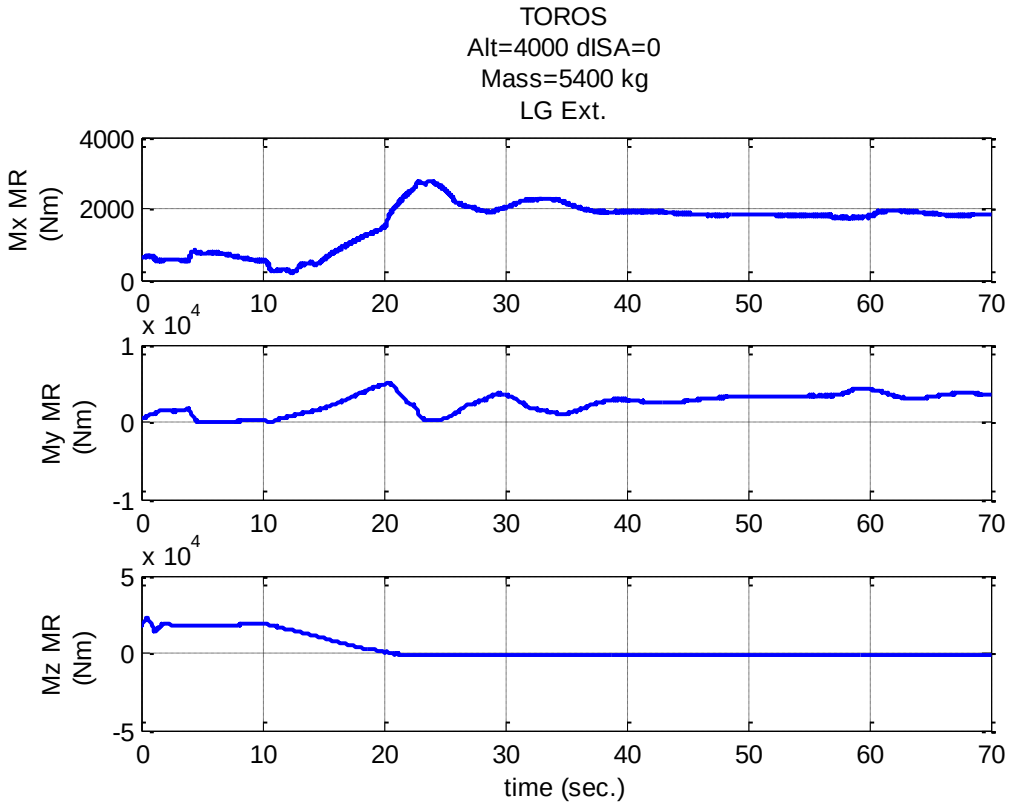

Figure 26 Moments of the Autorotation Maneuver

CHAPTER 3

AEROELASTIC BEAM-BLADE MODEL WITH TORSIONAL FLEXIBILITY

3.1 Development of the Beam-Blade Model Including Torsional Flexibility

In the present study, finite element beam-blade model with torsional flexibility has been developed and integrated to the in house flight dynamics code. For discretizing the beam-blade, the beam is split into finite elements, and each beam element has two nodes with elastic twist degrees of freedom at each end. Between these nodes the elastic twist is interpolated by shape functions.

Possible deflections of a beam can be classified into four; torsional displacement, a rotation about the beam's longitudinal axes, axial displacement, compression or expansion of the beam along its longitudinal axis, and flexural displacements, deflection the beam in the out-of-plane (flapwise) and in the in-plane (leadwise) directions. In this thesis, helicopter blade model is made flexible by including only torsional degree of freedom, and the Euler Bernoulli beam model is utilized to determine the mass and stiffness matrices associated with the torsional degree of freedom.

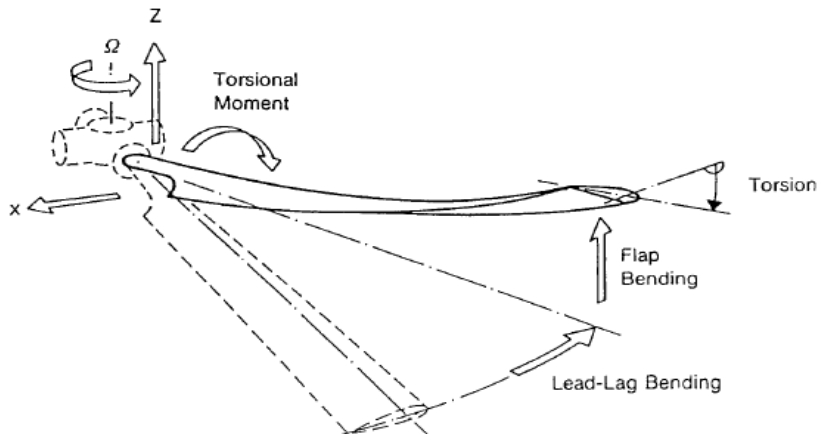

Figure 27 : Deflections of an Elastic Beam

For a beam element of length L, the relation between the torsional displacement in the beam and the nodal values of the torsional displacement is given by Eqn. (10).

$$\theta_{elastic}(x,t)=[a(x)]*\{q(t)\} \tag{10}$$

In Eqn.(10), a is the shape function matrix and q is the torsional nodal degree of freedom vector, and $\theta_{elastic}$ is the torsional displacement in the beam element.

Shape function matrix used in this study for torsional degree of freedom is given by Eqn.(11),

$$[a] = [1-\zeta \quad \zeta] \text{ and } \zeta = \frac{x}{L} \tag{11}$$

where L is the length of the beam element. Shape functions are defined in order to linearly interpolate the deformation within the element. Shape functions are normalized to use for element of any size by using a new local coordinate system. The ζ coordinate system is defined in a way that ζ=0 to 1 covers the entire length of the element. Using these shape functions, the torsional deformation within an element is interpolated as follows,

$$\theta_{elastic} = a_1 q_1 + a_2 q_2 \tag{12}$$

where q_1 and q_2 are the nodal torsional displacements of the element and a_1 and a_2 are shape functions. For instance, at the origin of the beam element ζ=0, $a_1 = 1$ and $a_2 = 0$. Hence, the torsional displacement at the origin of the element is $\theta_{elastic} = q_1$.

In this study shape functions are used to distribute the torsional deflection within an element as in Figure 28. Interpolations to blade element points are done after performing this distribution.

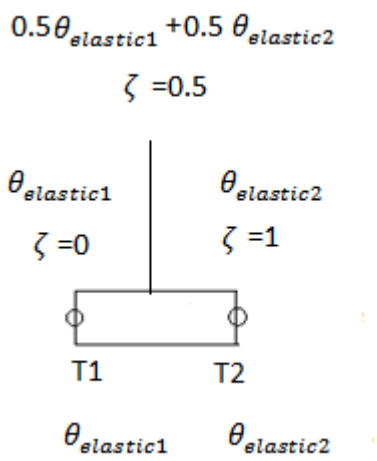

Figure 28 Distribution of Torsional Deflection Through an Element by the Help of Shape Functions

Mass and stiffness matrices for one beam element associated with the torsional deflection are calculated according to Eqn.(13),

$$[K]=\frac{GJ}{L}\begin{bmatrix}1 & -1\\ -1 & 1\end{bmatrix} \quad and \quad [M]=\frac{\rho JL}{6}\begin{bmatrix}2 & 1\\ 1 & 2\end{bmatrix} \tag{13}$$

where J is the polar moment of inertia, G is the shear rigidity and ρ is the density and L is the length of the element.

In the case of static loading, based on the theory of Euler Bernoulli beam theory, torsional deflection directly depends on the torsional moment T and the torsional rigidity term GJ, as given in Eqn (14),.

$$\frac{d\theta_{elastic}(x)}{dx}=\frac{T(x)}{GJ(x)} \tag{14}$$

An example torsional stiffness matrix for a three-element beam, shown in

Figure 29, is given by Eqn. (15). Here it is assumed that each beam element has the same length.

$$\frac{1}{L} * \begin{bmatrix} GJ_1 & -GJ_1 & 0 & 0 \\ -GJ_1 & GJ_1+GJ_2 & -GJ_2 & 0 \\ 0 & -GJ_2 & Gj_2+GJ_3 & -GJ_3 \\ 0 & 0 & -GJ_3 & GJ_3 \end{bmatrix} \begin{bmatrix} \theta_{elastic_1} \\ \theta_{elastic_2} \\ \theta_{elastic_3} \\ \theta_{elastic_4} \end{bmatrix} = \begin{bmatrix} T_1 \\ T_2 \\ T_3 \\ T_4 \end{bmatrix} \tag{15}$$

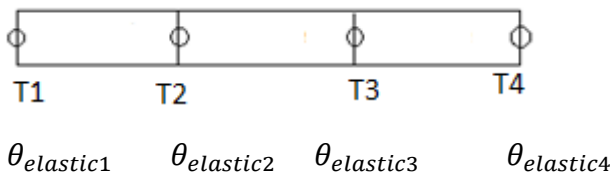

Figure 29 A Simple Three-Element Beam and with Torsional Degrees of Freedom Defined

The size of the matrix changes according to the number of beam elements used to model the beam blade. Torsional stiffness matrix for n-1 number of beam elements is given by Eqn (16),.

$$\frac{\begin{bmatrix} GJ_1 & -GJ_1 & 0 & & & & \\ -GJ_1 & GJ_1 + GJ_2 & -GJ_2 & \cdots & & 0 & \\ 0 & -GJ_2 & GJ_2 + GJ_3 & & & & \\ & \vdots & & \ddots & & \vdots & \\ & & & & GJ_{n-1} + GJ_{n-2} & -GJ_{n-2} & 0 \\ & 0 & & \cdots & -GJ_{n-2} & GJ_{n-1} + GJ_n & -GJ_n \\ & & & & 0 & -GJ_n & GJ_n \end{bmatrix} \frac{1}{L}}{\begin{bmatrix} \theta_{elastic_1} \\ \theta_{elastic_2} \\ \theta_{elastic_3} \\ \\ \\ \theta_{elastic_n} \end{bmatrix} = \begin{bmatrix} T_1 \\ T_2 \\ T_3 \\ \\ \\ T_n \end{bmatrix}} \tag{16}$$

In Figure 31 blade element nodes and finite element nodes taken on the blade is shown. The blade is modelled with a 6 beam finite elements and 20 number of blade elements. Interpolation is done through these points to solve equations of motions. Pitch angle of the blade is calculated at finite element points and equations of motions are solved at these points to find the elastic pitch angle. Inertial loads are also calculated directly at finite element points. Hence, aerodynamic force and moments that are initially calculated at blade element points are interpolated to these finite element points. At the end of interpolation, the aerodynamic loads effective on each finite element section are known and these loads are used in the equation of motion after combining with the inertial loads.

Pitch angle at a blade section is a combination of the collective (θ_0), cyclic (θ_{1c}, θ_{1s}) and the elastic deflection $\theta_{elastic}$ in the torsional direction as given in Eqn. (19) where the azimuth angle ψ is given by Ωt,

$$\theta_{total}(x,t)=\theta_{elastic}(\mathrm{x,t})+\theta_0+\theta_{1c}*cos(\psi)+\theta_{1s}*sin(\psi) \qquad (19)$$

3.2 Aerodynamic and Inertial Load Calculation

Aerodynamic and inertial loads from each segment, which are the sections where the forces are preferred to be calculated through blade, are used in load calculation. Load calculation is an important part of the study since the control system, rotor dynamics and aerodynamics, engine dynamics, blade dynamics hence the whole helicopter dynamics is linked very closely to the blade loads Figure 32 gives the flowchart of the calculation process of the aerodynamic loads at blade element segments and inertial loads at finite element segments.

From Figure 32, it is seen that segment velocities and pitch angles are used in the calculation of segment angle of attack and this angle of attack together with the Mach number is used in the determination of lift and drag coefficient values from look-up tables. After the determination of aerodynamic coefficients, segment aerodynamic loads are calculated.

At the same time inertial loads are calculated at each segment with finite element method. Throughout this chapter aerodynamic load calculation at blade element points, inertial load calculation at finite element points and integration of these loads at finite element points will be explained.

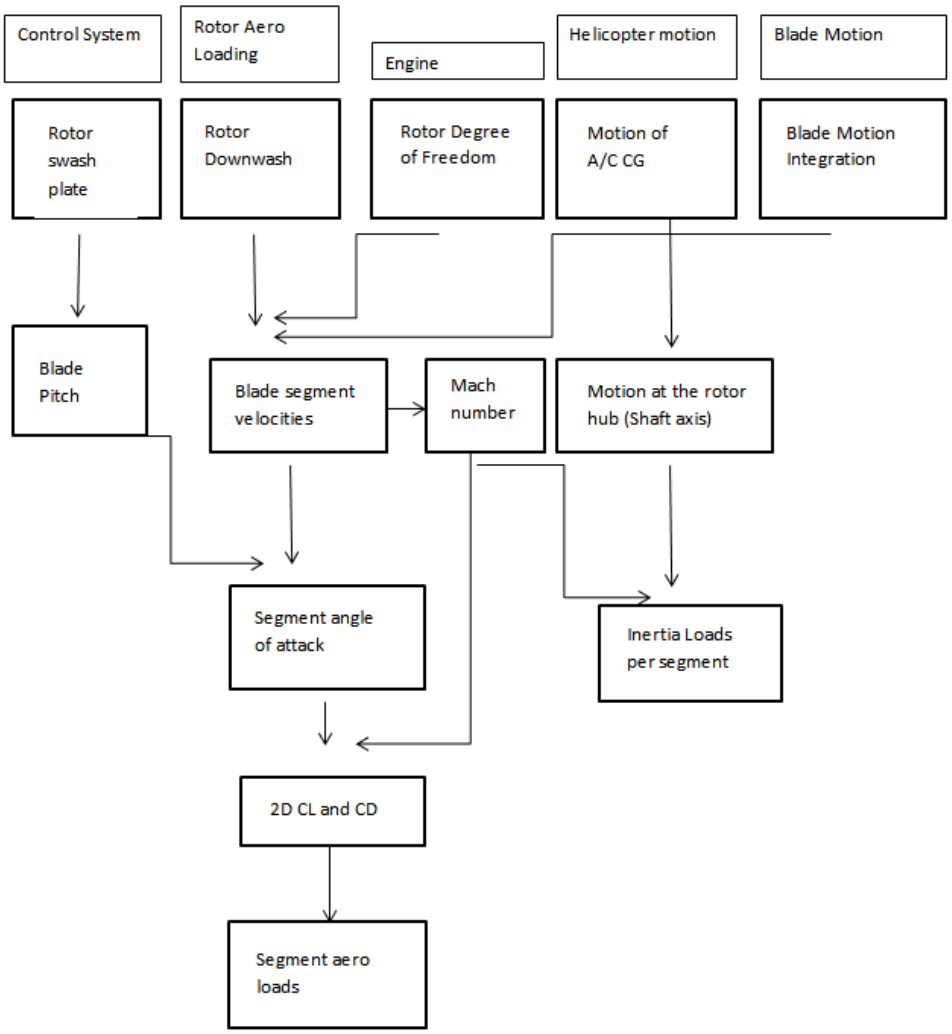

Figure 32 Flowchart of the Calculation Process of Aerodynamic Segment and Inertial Segment Loads

3.2.1 Calculation of the Aerodynamic Loads by the Blade Element Method (BEM)

Blade element method is used for the aerodynamic force and moment calculation by dividing blade into sections as in the finite element method, but these sections differ from finite element nodes and mainly more points are used compared to the finite element method. The main reason of dividing blade into sections is that different airfoils can be used through the blade and also the blade geometry changes along the blade span. Therefore, lift and drag forces are calculated at many points to achieve accurate modeling.

In forward flight there are velocity differences on the rotating blade. The main reason of this velocity difference is the translational and rotational velocity of the rotor.

Basic blade geometry is given in Figure 33. *x* axis is along the blade radius *R*, y axis is along the blade chord, c_{tip} denotes the chord length at tip. Hinge offset is denoted with e and r is the distance from hub.

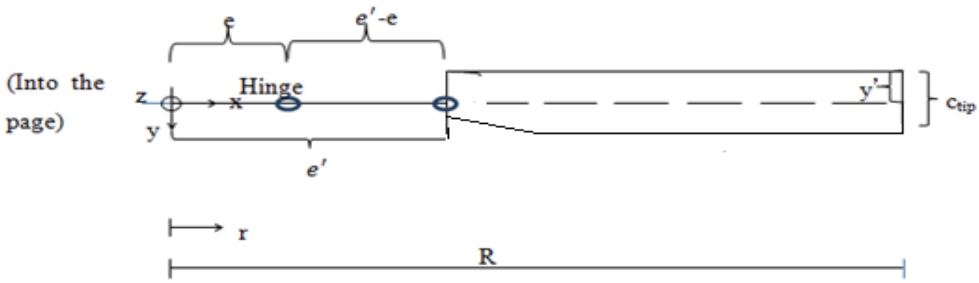

Figure 33 Blade Geometry Used in Simulation Tool

Different axis systems should be defined for a blade because of the lead-lag, flapping and feathering motion of blade (rotation of blade about three axis (β,δ,θ)), rotational velocity of rotor with Ω and the hinge offset. Different axis systems are used in the calculation of sectional velocities and accelerations which in turn are used in the calculation of sectional aerodynamic forces and moments. The order of axis

transformation is from shaft to main rotor hub axis with T_ψ, then from the hub axis to the lead-lag axis with the transformation matrix T_δ and from the lead-lag axis to the flap axis with T_β. After the lead-lag and flap transformations, the axis system reached is the blade axis. Then pitching, θ transformation is needed to reach sectional/local axis system to calculate local forces and moments. After the calculation of local forces and moments, in order to calculate the hub forces, back transformation should be done. Representation of different axis systems through the blade and sectional force representation again on the in house simulation tool blade is given in Figure 34.

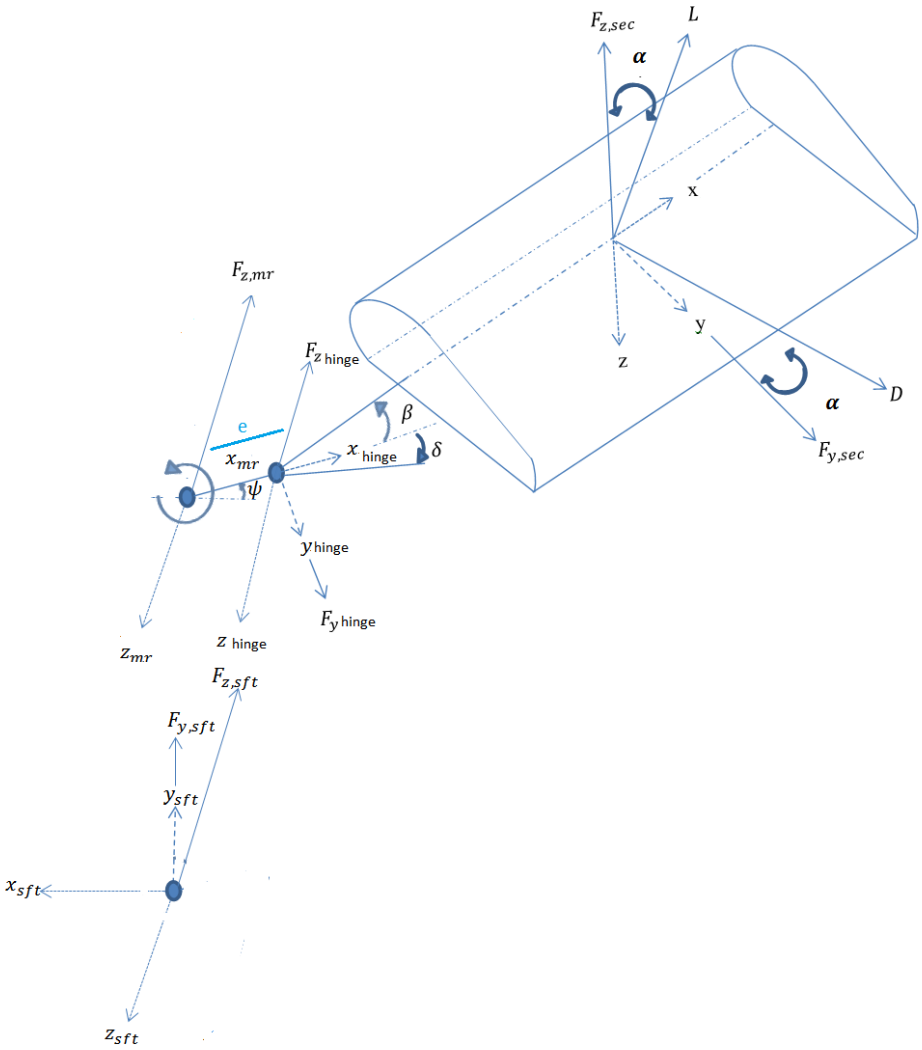

Figure 34 Representation of Different Axes Systems in the Simulation Tool Blade

The difference between the hub axis and shaft axis is the rotational velocity of the rotor. The shaft *x* axis is always directed to the front of the helicopter. The hub *x* axis is always directed to the blade which is rotating with ψ, hinge axis is the same with hub axis in terms of directions but there is hinge offset *e*. After the hinge axis, lead lag flap and feathering axes are introduced because of the blade motion.

V_{mr} is the main rotor hub translational velocity and V_{sft} is the shaft axis translational velocity and T_ψ is the transformation matrix from the shaft axis to the main rotor hub axis,

$$V_{mr} = T_\psi * V_{sft} \tag{20}$$

where

$$T_\psi = \begin{bmatrix} -\cos(\psi) & \sin(\psi) & 0 \\ -\sin(\psi) & -\cos(\psi) & 0 \\ 0 & 0 & 1 \end{bmatrix} \tag{21}$$

Rotational velocity of the main rotor hub, ω_{mr} is related to the shaft axis rotational velocity ω_{sft} which includes the roll rate, p_{sft}, the pitch rate , q_{sft} and the yaw rate r_{sft} of the shaft and the rotor RPM, Ω

$$\omega_{mr} = T_\psi * \left[\omega_{sft} + \begin{Bmatrix} 0 \\ 0 \\ -\Omega \end{Bmatrix}\right] \tag{22}$$

Translational velocity at the hinge is calculated from the translational velocity at the hub and the translational velocity coming from hinge offset as in Eqn. (23).

$$V_{hinge} = V_{mr} + \omega_{mr} \times \begin{Bmatrix} e \\ 0 \\ 0 \end{Bmatrix} \tag{23}$$

Blade leads and lags which is the lead-lag motion and the transformation matrix due to this motion is T_δ,

$$T_\delta = \begin{bmatrix} \cos(\delta) & \sin(\delta) & 0 \\ -\sin(\delta) & \cos(\delta) & 0 \\ 0 & 0 & 1 \end{bmatrix} \tag{24}$$

The blade at the same time flaps and flapping equation is given in Eqn (25)

$$\beta = \beta_0 + \beta_{1c} cos(\psi) + \beta_{1s} sin(\psi) \tag{25}$$

The transformation matrix as a result of this flapping motion is given by Eqn.(26).

$$T_\beta = \begin{bmatrix} \cos(\beta) & 0 & -\sin(\beta) \\ 0 & 1 & 0 \\ \sin(\beta) & 0 & \cos(\beta) \end{bmatrix} \tag{26}$$

From the main rotor to the blade axis, blade both flaps and lead-lags so the combined transformation matrix is,

$$T_{\delta\beta} = T_\beta T_\delta \tag{27}$$

$$C_{feat_{flap}} = \begin{bmatrix} 1 & 0 & 0 \\ 0 & \cos(\theta) & \sin(\theta) \\ 0 & -\sin(\theta) & \cos(\theta) \end{bmatrix} \tag{28}$$

where $T_{\delta\beta}$ is the transformation matrix from the main rotor to the blade axis**.** By the help of this matrix velocity on blade (V_{bld}) can be found as shown in Eqn.(29) and the rotational velocity on blade, ω_{bld} in Eqn.(30). It should be noted that V_{bld} is the translational velocity of blade axis which is at the hinge and formed after the blade lead-lags, flaps and rigidly feathers.

$$V_{bld} = C_{feat_{flap}} * T_{\delta\beta} * V_{hinge} \tag{29}$$

$$\omega_{bld} = C_{feat_{flap}} * T_{\delta\beta} * \omega_h + \begin{bmatrix} \dot{\theta} \\ 0 \\ 0 \end{bmatrix} \tag{30}$$

where the $\dot{\theta}$ is the rigid pitch angle.

Translational velocity at each blade element section is calculated from the translational velocity of blade V_{bld}, rotational velocity of blade ω_{bld} which creates a translational velocity in the y direction of the blade, and the inflow coefficients, uniform inflow coefficient (λ_0) lateral inflow coefficient, (λ_{1s}) and longitudinal inflow coefficient (λ_{1c}).

$$V_{sec} = V_{bld} + (\lambda_0 \sin(\beta_0))\hat{\imath} + ((r_{bem} - e)\mathrm{x}\omega_{bldz})\hat{\jmath} + [-[\lambda_0 \cos(\beta_0) + \frac{r}{R}(\lambda_{1c} cos(\psi) + \lambda_{1s} sin(\psi)] \cdot \Omega R]\hat{k} \tag{31}$$

V_{sec} is the velocity at the blade axes, which is the axis formed after blade flaps, lags and feathers rigidly. The calculated translational velocity at each section is then used in the calculation of the lift and drag forces. Here r vector in x-y-z directions for all sections is given by

$$r = \begin{bmatrix} (r_{bem} - e) \\ 0 \\ 0 \end{bmatrix} \tag{32}$$

where r_{bem} is the cg of the blade element sections in the x direction along the blade span and from hub.

Aeroelastic deformations of the rotor blade affect the helicopter performance, airloads, and the vibration. Elastic deformation about the feathering plane is known as the torsional deformation, $\theta_{elastic}$. Pitch angle, θ is one of the most influential parameter on the aerodynamics since it contributes to the angle of attack (α) of the sections of the rotor blade, as shown in Figure 35. Hence elastic deformation $\theta_{elastic}$ should be included in the effective angle of attack calculation. The angle of attack is the most important parameter in the production of lift along the span of the rotor blade. Since elastic torsional deformation has an effect on the lift production through angle of attack, aerodynamic force and moments should be recalculated with the elastic blade model including torsional flexibility.

The effective angle of attack α at the blade sections is,

$$\alpha = \phi + \theta_{tw} + \theta_{elastic} \tag{33}$$

where θ_{tw} is the twist angle changing through blade, ϕ is the induced angle of attack. $\theta_{elastic}$ is the elastic twist again changing from section to section.

The induced angle of attack ϕ is given in Figure 35 as,

$$\phi = arctan\left(\frac{U_p}{U_T}\right) \tag{34}$$

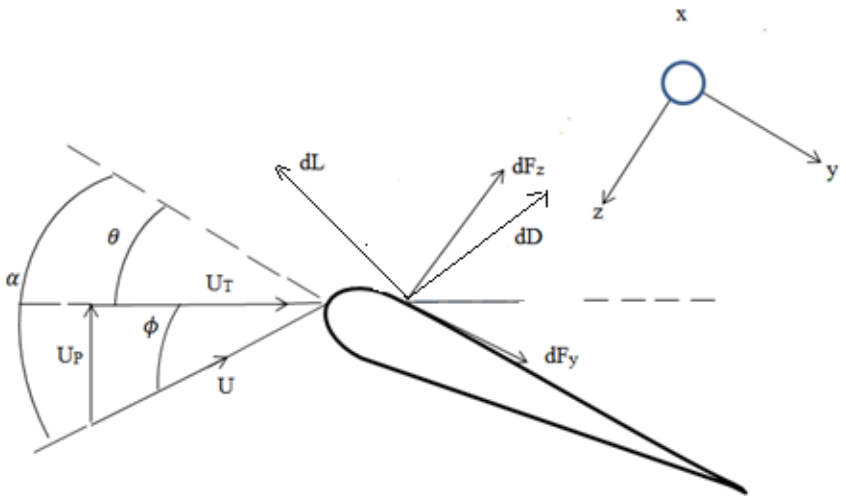

Figure 35 Geometric Angle Representation on an Airfoil

Lastly geometric angle of attack is the difference between angle of attack and induced angle of attack,

$$\alpha_{geo} = \theta_{tw} + \theta_{elastic} \tag{35}$$

For the aerodynamic force and moment calculation at each local section a new axis transformation is needed to represent this local axis. This transformation matrix includes the dihedral, sweep angle of blade and the geometric angle of attack, and it is given by,

$$C_{loc_{bld}} = \begin{bmatrix} 1 & 0 & 0 \\ 0 & \cos(a_{geo}) & \sin(a_{geo}) \\ 0 & -\sin(a_{geo}) & \cos(a_{geo}) \end{bmatrix} * T_{dihed\&sweep} \tag{36}$$

$$V_{sec_{loc}} = C_{loc_{bld}} * V_{sec} \tag{37}$$

Transformation matrix is calculated with geometric angle of attack and the main reason of this is that the, transformation matrix is independent from the flow direction.

The directions and geometric relations can be found in the Figure 35 and Figure 34 related to the calculation of the lift and the drag forces. Lift is always perpendicular to the flow and drag is perpendicular to the lift force.

Aerodynamic coefficients including lift coefficient,C_l, drag coefficient, C_d and pitching moment coefficient $C_{m,x}$ values, are given as aerodynamic tables which are based on Mach numbers and angle of attacks. Lift coefficients at each angle of attack is found from these tables using Mach number and angle of attack interpolation. The effective angle of attack is used during these interpolations.

In order to get correct values from tables tip loss effect on lift coefficient should be taken into account. By using the lift and drag coefficients local lift and local drag on the blade is calculated in Eqn. (38) and Eqn. (39). Following the calculation of the sectional lift and the drag, force on the section, force in the z direction is calculated by, Eqn.(40), and the force on the blade section in the y direction is calculated by, Eqn. (41).

$$dL = -0.5 \cdot \rho \cdot V^2{}_{sec_{loc}} \cdot C_l(\alpha, Mach) \cdot dA \tag{38}$$

$$dD = 0.5 \cdot \rho \cdot V^2{}_{sec_{loc}} \cdot C_d(\alpha, Mach) \cdot dA \tag{39}$$

$$F_{\mathrm{z,sec}} = dL \cdot cos(\alpha) - dD \cdot sin(\alpha) \tag{40}$$

$$F_{y,sec} = dL \cdot sin(\alpha) + dD \cdot co\,s(\alpha) \tag{41}$$

Drag acting on the blade in radial (x), direction is $F_{x,sec}$,

$$F_{x,sec} = 0.5 \cdot \rho \cdot V^2{}_{sec_{loc}} \cdot C_x(\alpha, Mach) \cdot dA \tag{42}$$

where C_x is the radial drag aerodynamic coefficient.

$$F_{sec} = \begin{bmatrix} F_{x,sec} \\ F_{y,sec} \\ F_{z,sec} \end{bmatrix} \tag{43}$$

For each blade segment after defining the force matrix, firstly moments at the blade root from these forces are calculated. Secondly, in addition to the root moment created by the forces, moments along the hinge due to hinge offset are added and the total moment and the torque on the main rotor are calculated.

Sectional forces are transformed back to the blade axis using the transformation matrix $C_{bld_{loc}}$, which is the transpose of $C_{loc_{bld}}$.

$$F_{bld} = C_{bld_{loc}} * F_{sec} \tag{44}$$

Moment at flapping hinge, axis (y) of blade, of each section at the blade root is given by,

$$M_{y,b} = (r_{bem} - e) * F_{z,bld} + M_{ybld} \tag{45}$$

where (r_{bem}-e) is the moment arm to blade root for every blade element force since r_{bem} is the x location of blade element points from hub and $F_{z,bld}$ is the force in blade axis z direction and M_{ybld} the aerodynamic moment in y direction.

Moment about lead-lag axis, z axis of blade, of each section at the root.

$$T_{z,b} = (r_{bem} - e) * F_{y,bld} + M_{zbld} \tag{46}$$

where $F_{y,bld}$ is the force in blade axis in the y direction and M_z the aerodynamic moment in the z direction. From these moments moment at the hinge can be found by adding the moment of the blade forces at the hinge due to the hinge offset.

During the calculation of the feathering moment, feathering moment coefficient $C_{M,x}$ is found from the look up tables for different angle of attack and Mach numbers. Feathering moments is then calculated from Eqn. (47),

$$FM_{local} = 0.5 \cdot \rho \cdot V^2{}_{sec_{loc}} \cdot C_{M,x} \cdot dA \tag{47}$$

$$FM = C_{bld\_loc} * \begin{bmatrix} FM_{local} \\ 0 \\ 0 \end{bmatrix} \tag{48}$$

where FM is the feathering moment at each section, $C_{M,x}$ is the feathering moment coefficient, c_x ·is the dimensional sectional chord, $V_{sec_{loc}}$ is the sectional velocity and C_{bld_loc} is the transformation matrix including blade sweep, dihedral angle and geometric angle of attack which is used in the back transformation from the local axis to the blade axis. This feathering moment will contribute to the finite element model as aerodynamic moment in torsional direction. This contribution will be in

finite element nodes so before the integration, aerodynamic feathering moment calculated at each blade element section is interpolated to finite element nodes. This procedure is as follows,

- The X direction CG's of blade element sections (r_{bem}) and the cg in x direction of finite element sections (r_{cg}) are compared.
- If $r_{bem} < r_{cg}$ and if the blade element boundaries of the current blade element section are completely in the boundaries of current finite element section aerodynamic moment of bem section is directly added to the feathering moment of the finite element nodes of current finite element section. This addition is done inversely by the distance ratio of aerodynamic node to finite element nodes.
- If the blade element section boundaries are in the boundary of more than one finite element section as in Figure 36 then,

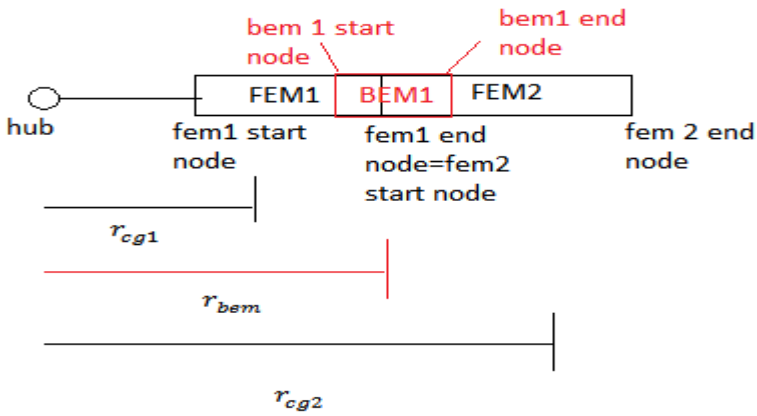

Figure 36 Blade Element Section in the Boundary of More than One Finite Element Section

- $First\ FE\ section\ aerodynamic\ moment\ contribution = \frac{FM_{local}}{length\ bem1\ section} * (bem1\ start\ node - fem1\ end\ node)$
- $Second\ FE\ section\ aerodynamic\ moment\ contribution = \frac{FM_{local}}{length\ bem\ section} * (bem1\ end\ node\ - fem2\ start\ node)$

And then these sectional aerodynamic moments distributed to the nodes of each section which is inversely proportional to the distance of the aerodynamic load center to finite element nodes of the section.

3.2.2 Calculation of Inertial Loads with Finite Element Method

The blade lead-lags and flaps from hinge and axis systems should be defined for each of the blade motions. After the flap motion blade feathers and this time another axis system should be defined from flap to feather axis.

Flapping axis is the blade axis defined after the blade lead-lags and flaps at the hinge and the blade feathers about the feathering axis in the rigid case. Blade axis is along the feathering axis which pitches with the pitch angle θ. Figure 37 shows the total pitch angle θ on a blade section and the formation of new axis with the feathering motion. The initial axis is the blade axis after flapping denoted with $\vec{\imath}$, $\vec{\jmath}$ and $\vec{k}$ and the final axis after feathering with $\vec{\imath'}$, $\vec{\jmath'}$ and $\vec{k'}$.

Transformation matrix from the flapping axis to the blade feathering axis is calculated using the pitch angle is given in Eqn. (49),

$$C_{feat_{flap}} = \begin{bmatrix} 1 & 0 & 0 \\ 0 & \cos(\theta) & \sin(\theta) \\ 0 & -\sin(\theta) & \cos(\theta) \end{bmatrix} \tag{49}$$

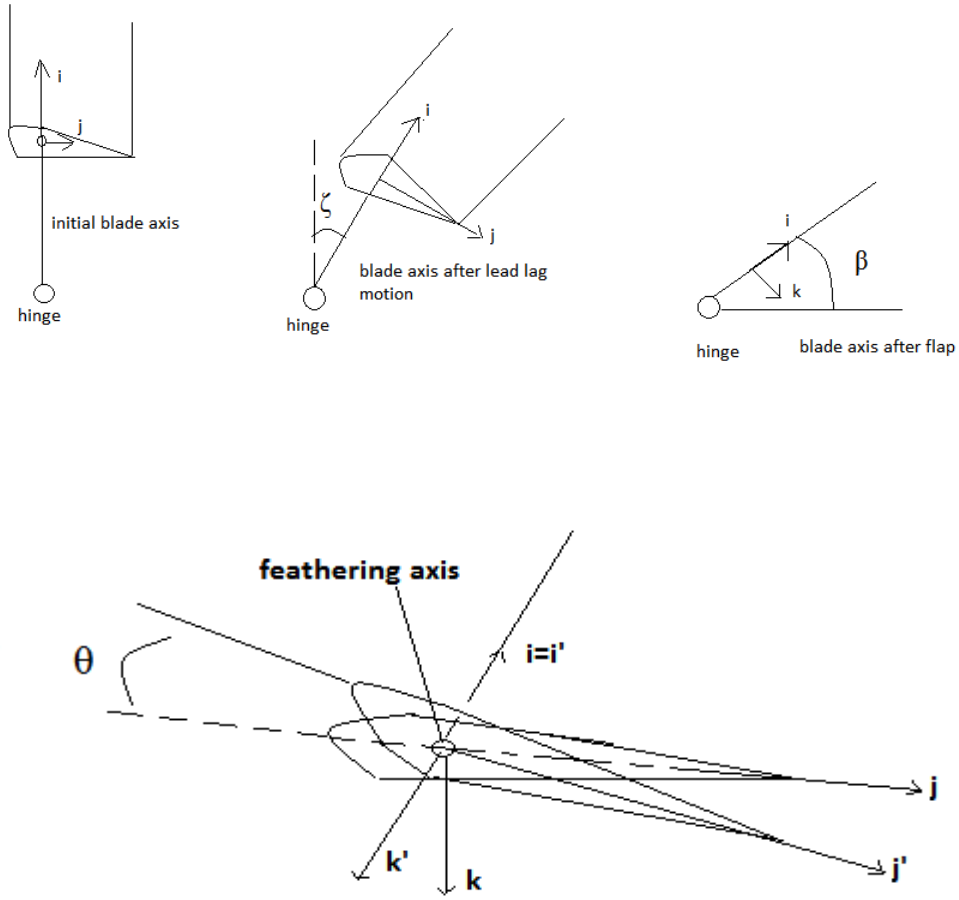

Figure 37 Feathering and blade axes

Hence the transformation matrix from the blade feathering axis to the flap axis is the transpose of Eqn. (49),

$$C_{flap_{feat}} = C^{\mathrm{T}}_{feat_{flap}} \tag{50}$$

The rotational velocity w_{flap}, rotational acceleration $\widetilde{w}_{flap}$, and the translational acceleration of blade a_{flap} in the flap axes are all transferred and calculated at the local feathering axis, which is the blade axis in Eqn. (51), Eqn. (53) and Eqn. (54).

$$w_{bld} = C_{feat_{flap}} * w_{flap} + \begin{bmatrix} \dot{\theta} \\ 0 \\ 0 \end{bmatrix} \tag{51}$$

where $w_{flap} = T_{\delta\beta} \cdot \omega_h$ is the rotational velocity of the flap axis given by the transformation of the hub rotational velocity, which includes the body angular velocities (p,q,r) and the rotational velocity of rotor, Ω, first to lead lag axis and then to the flap axis, and the total pitch angle is given by Eqn. (52)

$$\theta = \theta_0 + \theta_{1c} * cos(\psi) + \theta_{1s} * sin(\psi) \tag{52}$$

And $\dot{\theta} = \dot{\theta}_0 + \dot{\theta}_{1c} * cos(\psi) - \theta_{1c} * sin(\psi) * \Omega + \dot{\theta}_{1s} * sin(\psi) + \theta_{1s} * cos(\psi) * \Omega$

where Ω is the rotational speed of the rotor and $\psi = \Omega t$.

$$\widetilde{w}_{bld} = C_{feat_{flap}} * \widetilde{w}_{flap} + \dot{C}_{feat_{flap}} * w_{flap} + \begin{bmatrix} \ddot{\theta} \\ 0 \\ 0 \end{bmatrix} \tag{53}$$

$$a_{bld} = C_{feat_{flap}} * a_{flap} \tag{54}$$

From Eqn. (55) and Eqn. (56) feathering velocity and acceleration matrices are calculated.

$$\widetilde{w}_{bld} = \begin{bmatrix} 0 & -w_{z_{bld}} & w_{y_{bld}} \\ w_{z_{bld}} & 0 & -w_{x_{bld}} \\ -w_{y_{bld}} & w_{x_{bld}} & 0 \end{bmatrix} \tag{55}$$

$$\widetilde{\dot{w}}_{bld} = \begin{bmatrix} 0 & -\dot{w}_{z_{bld}} & \dot{w}_{y_{bld}} \\ \dot{w}_{z_{bld}} & 0 & \dot{w}_{x_{bld}} \\ -\dot{w}_{y_{bld}} & \dot{w}_{x_{bld}} & 0 \end{bmatrix} \tag{56}$$

Cg vector in x-y-z directions for all sections is given by Eqn. (57) where r_{cg} is the cg of the finite element section in the x direction along the blade span and ycg is the cg of all sections in the y direction, along the blade chord.

$$cg_{bld} = \begin{bmatrix} r_{cg} \\ ycg \\ 0 \end{bmatrix} \tag{57}$$

When the torsional flexibility is included, then the pitch angle is calculated as shown in Eqn.(58)

$$\theta_{total} = \theta + \theta_{elastic} \tag{58}$$

The blade lead-lags and flaps and transformation matrix from the flap axis to the blade feathering axis is written as in Eqn.(49) in the rigid case. In elastic case after the transformation from the flap axis to the blade feathering axis due to rigid pitch, one more transformation is done due to the elastic pitch. Hence the local translational and rotational velocities and accelerations are updated because of the elastic twist resulting from the elastic blade modeling. Different from the rigid blade, feathering angles, local velocity and accelerations are now calculated at more than one point for each finite element node along the blade at the new local elastic feathering axis.

The transformation matrix from rigid blade feathering axis to elastic blade feathering local axis is given.in Eqn.(59).

$$C_{bld_{feat\_elastic}} = \begin{bmatrix} 1 & 0 & 0 \\ 0 & \cos(\theta_{elastic}) & \sin(\theta_{elastic}) \\ 0 & -\sin(\theta_{elastic}) & \cos(\theta_{elastic}) \end{bmatrix} \tag{59}$$

$$\dot{C}_{bld_{feat\_elastic}} = \begin{bmatrix} 0 & 0 & 0 \\ 0 & -\sin(\theta_{elastic}) * \dot{\theta}_{elastic} & \cos(\theta_{elastic}) * \dot{\theta}_{elastic} \\ 0 & -\cos(\theta_{elastic}) * \dot{\theta}_{elastic} & -\sin(\theta_{elastic}) * \dot{\theta}_{elastic} \end{bmatrix} \tag{60}$$

$$w_{bld_{elastic}} = C_{bld_{feat\_elastic}} * w_{bld} + \begin{bmatrix} \dot{\theta}_{elastic} \\ 0 \\ 0 \end{bmatrix} \tag{61}$$

$$\dot{w}_{bld_{elastic}} = C_{bld_{feat\_elastic}} * \dot{w}_{bld} + \dot{C}_{bld_{feat\_elastic}} * w_{bld} + \begin{bmatrix} \ddot{\theta}_{elastic} \\ 0 \\ 0 \end{bmatrix} \tag{62}$$

$$a_{bld_{elastic}} = C_{bld_{feat\_elastic}} * a_{bld} \tag{63}$$

And then $\widetilde{w}_{feat\_elastic}$ and $\breve{\dot{w}}_{feat\_elastic}$ is calculated once again using the matrices as in and Eqn. (55) Eqn. (56) which are used in the inertial force and moment calculations. The generalized inertial force equation is given as,

$$InertialForce = m_{bld} * (\ddot{r} + w \text{ x } w \text{ x } r + \dot{w} \text{ x } r) \tag{64}$$

which is rewritten using the notations of the study,

$$= m_{bld} * \left(a_{bld_{elastic}} + w_{bld_{elastic}} \text{ x } w_{bld_{elastic}} \text{ x } r + \dot{w}_{bld_{elastic}} \text{x } r\right)$$

Where m_{bld} is the mass distribution of blade, r =cg_{bld} is the cg distribution of blade finite element sections in x-y and z axes given in Eqn. (57).

$$\dot{w}_{bld_{elastic}} \text{ x } r = \widetilde{\dot{w}}_{bld_{elastic}} * [cg_{bld}] \tag{65}$$

$$\begin{aligned} &w_{bld_{elastic}} \text{ x } w_{bld_{elastic}} \text{ x } r \\ &\quad = \widetilde{w}_{bld_{elastic}} * w_{bld_{elastic}} \text{ x } r \end{aligned} \tag{66}$$

$$w_{bld_{elastic}} \text{ x } r = \widetilde{w}_{bld_{elastic}} * [cg_{bld}] \tag{67}$$

Hence,

$$\begin{aligned} &Inertial\ Moment \\ &\quad = I_{vec} * \dot{w}_{bld_{elastic}} + w_{bld_{elastic}} \text{x} \left(I_{vec} * w_{bld_{elastic}}\right) \\ &\quad + \widetilde{cg}_{bld} * InertialForce \end{aligned} \tag{68}$$

where,

$$\begin{aligned} &w_{bld_{elastic}} \text{ x } I_{vec} * w_{bld_{elastic}} \\ &\quad = \widetilde{w}_{bld_{elastic}} * \left(I_{vec} * w_{bld_{elastic}}\right) \end{aligned} \tag{69}$$

where I_{vec} is the inertia matrix of the vector and where product of inertias are zero hence a diagonal matrix of blade sections in x-y and z direction.

In torsional direction inertial moment, $Inertial\ Moment_x$ is calculated from Eqn. (70),

$$Inertial\ Moment = \begin{bmatrix} I_{vecx} * \dot{w}_{x_{feat}} \\ I_{vecy} * \dot{w}_{y_{feat}} \\ I_{vecz} * \dot{w}_{z_{feat}} \end{bmatrix} + \begin{bmatrix} 0 & -\dot{w}_{z_{feat}} & \dot{w}_{y_{feat}} \\ \dot{w}_{z_{feat}} & 0 & -\dot{w}_{x_{feat}} \\ -\dot{w}_{y_{feat}} & \dot{w}_{x_{feat}} & 0 \end{bmatrix} * \begin{bmatrix} I_{vecx} * w_{x_{feat}} \\ I_{vecy} * w_{y_{feat}} \\ I_{vecz} * w_{z_{feat}} \end{bmatrix} \tag{70}$$

$$Inertial\ Moment_x = I_{vecx} * \dot{w}_{x_{feat}} - \dot{w}_{z_{feat}} * I_{vecy} * w_{y_{feat}} + \dot{w}_{y_{feat}} * I_{vecz} * w_{z_{feat}} \tag{71}$$

Calculated inertial moment is transformed back to the blade coordinate from the local coordinate using $C_{bld_{feat\_elastic}}$ in Eqn. (59).

3.3 Integration of Aerodynamic and Inertial Moments to Aeroelastic Solution

In determining the response to maneuver, pitching acceleration is calculated from the feathering aerodynamic moment and inertial moment in the torsional direction. where

In order to solve for elastic pitching acceleration, matrix system in Eqn. (15) should be solved. The matrix system set after the calculation of inertial and aerodynamic moments in feathering direction is,

K is the integrated stiffness matrix, J is the inertia in x direction in kgm^2

$$\begin{bmatrix} GJ_1 & -GJ_1 & 0 & & & & \\ -GJ_1 & GJ_1+GJ_2 & -GJ_2 & \cdots & & 0 & \\ 0 & -GJ_2 & GJ_2+GJ_3 & & & & \\ & \vdots & & \ddots & & \vdots & \\ & & & & GJ_{n-1}+GJ_{n-2} & -GJ_{n-2} & 0 \\ & 0 & & \cdots & -GJ_{n-2} & GJ_{n-1}+GJ_n & -GJ_n \\ & & & & 0 & -GJ_n & GJ_n \end{bmatrix} * \frac{1}{L}$$

$$\begin{bmatrix} \theta_{elastic_1} \\ \theta_{elastic_2} \\ \theta_{elastic_3} \\ \\ \\ \theta_{elastic_n} \end{bmatrix} + \begin{bmatrix} \ddot{\theta}_{elastic1} * J_1 \\ \ddot{\theta}_{elastic2} * J_2 \\ \ddot{\theta}_{elastic3} * J_3 \\ \\ \\ \ddot{\theta}_{elasticn} * J_n \end{bmatrix} = \begin{bmatrix} (FM+Inertial\ Moment_x)_1 \\ (FM+Inertial\ Moment_x)_2 \\ (FM+Inertial\ Moment_x)_3 \\ \\ \\ (FM+Inertial\ Moment_x)_n \end{bmatrix} \tag{72}$$

where $\theta_{elastic}$, polar moment of inertias, J, length of each element, L, and sectional aerodynamic and inertial moments are all known. It should be noted that $\theta_{elastic}$ is known from the previous time step solution and it is initially zero at the very beginning. FM is from Eqn. (47), $Inertial\ Moment_x$ is from Eqn. (68),

Pitch angle is found from the integration of pitching acceleration,

$$\int \ddot{\theta}_{elastic} = \int \dot{\theta}_{elastic} = \theta_{elastic} \tag{73}$$

This integration is done in multi body coordinate this coordinate is the coordinate that defines tip path plane and used in flapping, lead-lag and feathering motion.

Tip Path Plane Dynamics

The asymmetry of the aerodynamic environment in forward flight, which is due to the combination of forward velocity and rotor rotation, causes the blade loads and the motion to depend on the azimuthal position, ψ. For steady state problems, the blade motion at a given azimuth must be the same hence blade loads and motion is periodic with respect to the azimuth. Rotor blade behavior is periodic with a fundamental frequency Ω and period T ($T=\frac{2\pi}{\Omega}$). Since periodic functions can be represented by Fourier series, the steady state flap motion is described by,

$$\beta(\psi) = \beta_0 + \beta_{1c}\, cos(\psi) + \beta_{1s}\, sin(\psi) + \beta_{2c}\, cos(2\psi) + \beta_{2s}\, sin(2\psi) + \cdots \tag{74}$$

where the periodic function, $\beta(\psi)$, is defined by the harmonics β_0, β_{1c}, β_{1s} and so on. Generally only the lowest few harmonics are required to adequately describe the rotor motion. The harmonics are obtained through Eqn. (75) to (78),

$$\beta_0 = \frac{1}{2\pi}\int_0^{2\pi} \beta\, d\psi \tag{75}$$

$$\beta_{nc} = \frac{1}{\pi}\int_0^{2\pi} \beta\, \cos(n\psi) d\psi \tag{76}$$

$$\beta_{ns} = \frac{1}{\pi}\int_0^{2\pi} \beta\, \sin(n\psi) d\psi \tag{77}$$

For a 5 bladed rotor multi-body coordinate corresponding to individual body coordinate becomes,

$$\beta_I = \{\beta_1, \beta_2, \beta_3, \beta_4, \beta_5\} \text{ and } \beta_M = \{\beta_0, \beta_{1c}, \beta_{1s}, \beta_{2c}, \beta_{2s}\} \tag{78}$$

Where $\{\beta_1, \beta_2, \beta_3, \beta_4, \beta_5\}$ are the flapping angles of the each 5 blade and is called flapping in individual body coordinate and $\{\beta_0, \beta_{1c}, \beta_{1s}, \beta_{2c}, \beta_{2s}\}$ are the flapping of tip path plane and called flapping in multi-body coordinate.

The zero harmonic, β_0 is the coning angle when $\beta = \beta_0$, flap motion is independent of azimuth. The combination of harmonics β_0, β_{1c}, β_{1s} forms a cone that has a lateral and longitudinal tilt. The circular path described by the blade tips still lie in a plane called tip path plane. The orientation of the tip path plane relative to the reference plane is given by β_{1c}, β_{1s} as shown in Figure 38. The higher harmonics of flap motion produce a distortion of the tip path plane which are small.

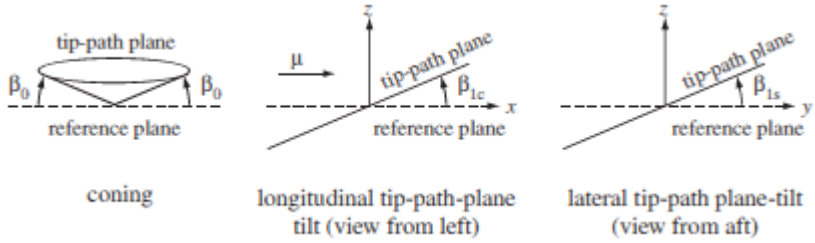

Figure 38 Tip Path Plane [15]

To summarize, thrust vector can be thought as a vector perpendicular to tip path plane, so by tilting this plane and changing the direction of thrust vector helicopter can move back, forward or left and right. This motion of tip path plane is defined by multi body coordinates, coning lateral and longitudinal flapping angles defining the total cone angle and lateral and longitudinal tilt angle of tip path plane. Individual body coordinates are formed from the motion of each individual blade corresponding to those multi body coordinates.

3.4 Static Solution of Beam Blade and Comparison with Dymore

In finite element beam, properties are defined at several points called sections or segments on blade, the stiffness, mass, inertia and cg of the sections are defined throughout the blade and calculations are done for each section. The non-dimensional sectional properties of blade are given in Figure 39 to Figure 41.

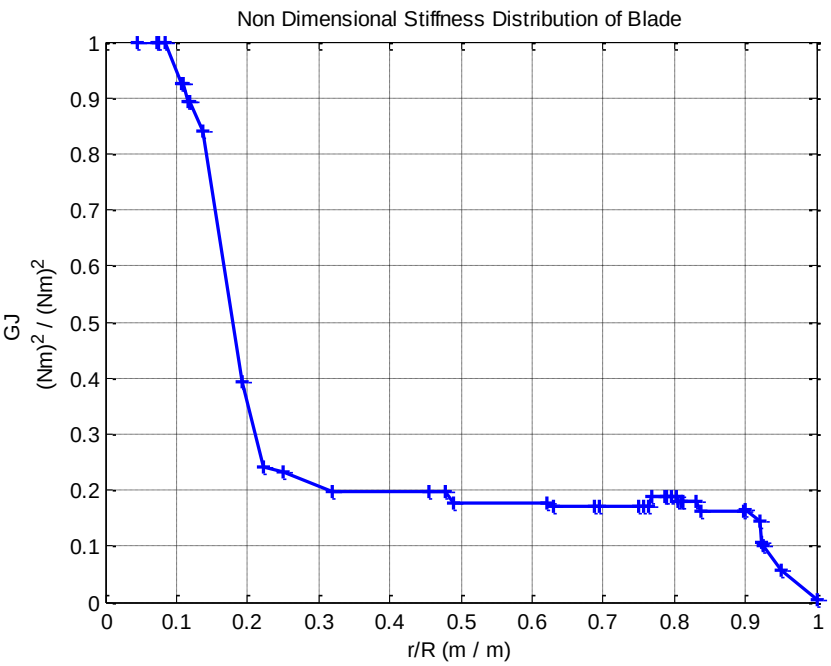

Figure 39 Non Dimensional Stiffness Distribution of the Blade

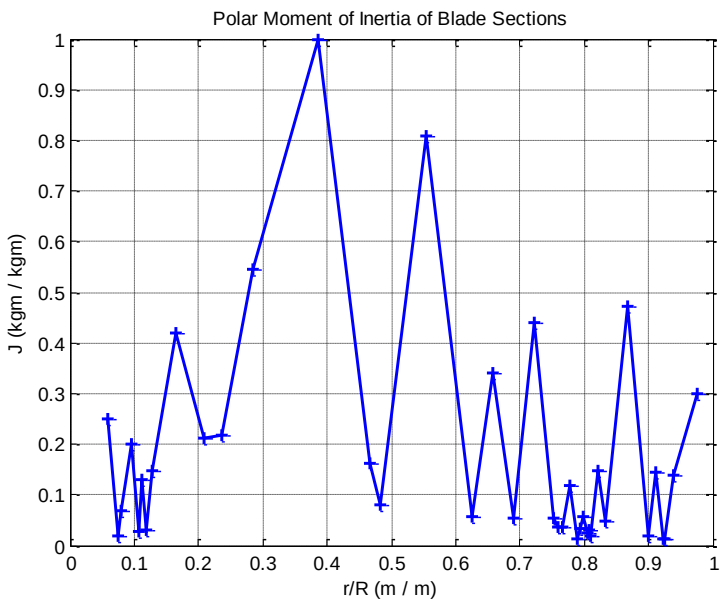

Figure 40 Non Dimensional Polar Moment of Inertia Distribution of the Blade

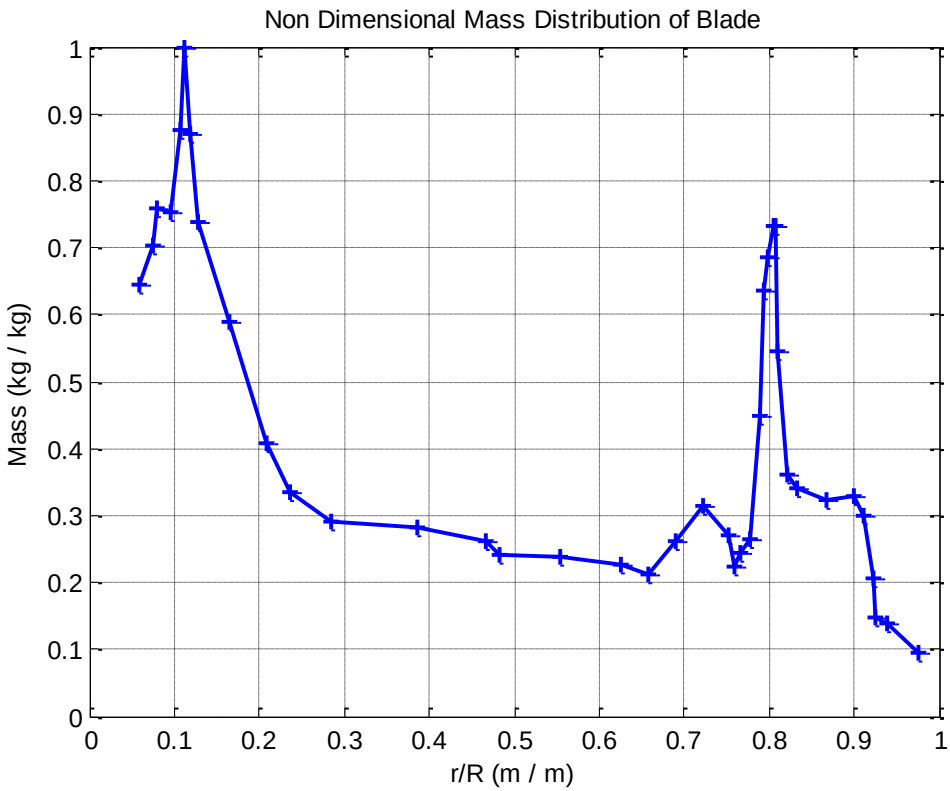

Figure 41 Non Dimensional Mass Distribution of Blade

The static elastic solution of beam blade in wind tunnel trim is compared with Dymore [19] results in order to see the accuracy of modeling. Wind tunnel trim is a special trim where there is only rotor component and like a wind tunnel analysis rotor is fixed from the shaft. Wind tunnel trim is preferred in the comparison study performed with Dymore since Dymore cannot trim the whole helicopter. In Dymore, there is only isolated rotor which is fixed from the shaft and control angles are given to the rotor and which is eventually trimmed. In Figure 42 comparison of the elastic torsional deflection through blade calculated by TOROS and Dymore is given. The comparison is given for hover and 140 knot forward flight. The analyses are done with three different number of finite element node selection, hence it gives an idea about effect of node number on results.

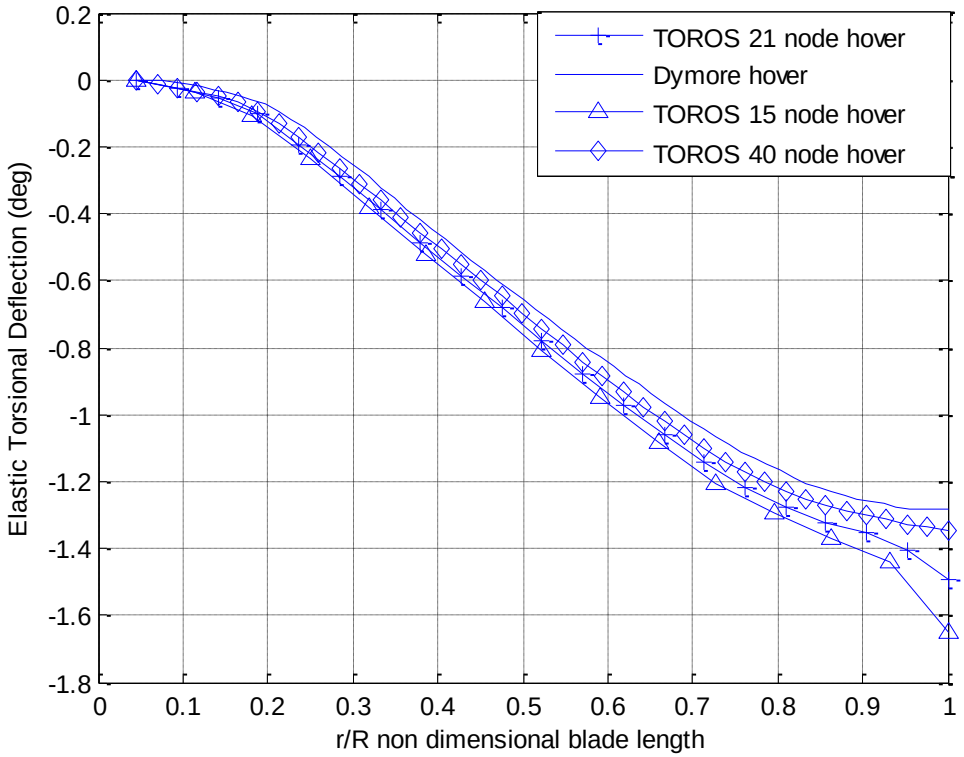

Figure 42 Comparison of TOROS Hover Elastic Torsional Deflection Through Blade with Dymore

The tip twist predicted by Dymore at hover is -1.28 degree, this value is -1.34 degree for the 40 node solution,-1.5 degree for the 21 node solution and -1.65 degree for the 15 node solution performed by the elastic blade model in TOROS. The effect of node number on the elastic deflection is small up to the tip of the blade. The variation of deflection with node number is less than 0.1 degree up to the tip node. At the tip deflection there is 0.3 degree difference between the 15 node and 40 node FE solutions of TOROS. Hence it can be concluded that 15 nodes represent the hover results well enough up to the tip node. As the number of nodes increase and become 40, the hover results of TOROS get closer to Dymore results. Especially, the tip deflection becomes smoother and zero slope condition is nearly satisfied.

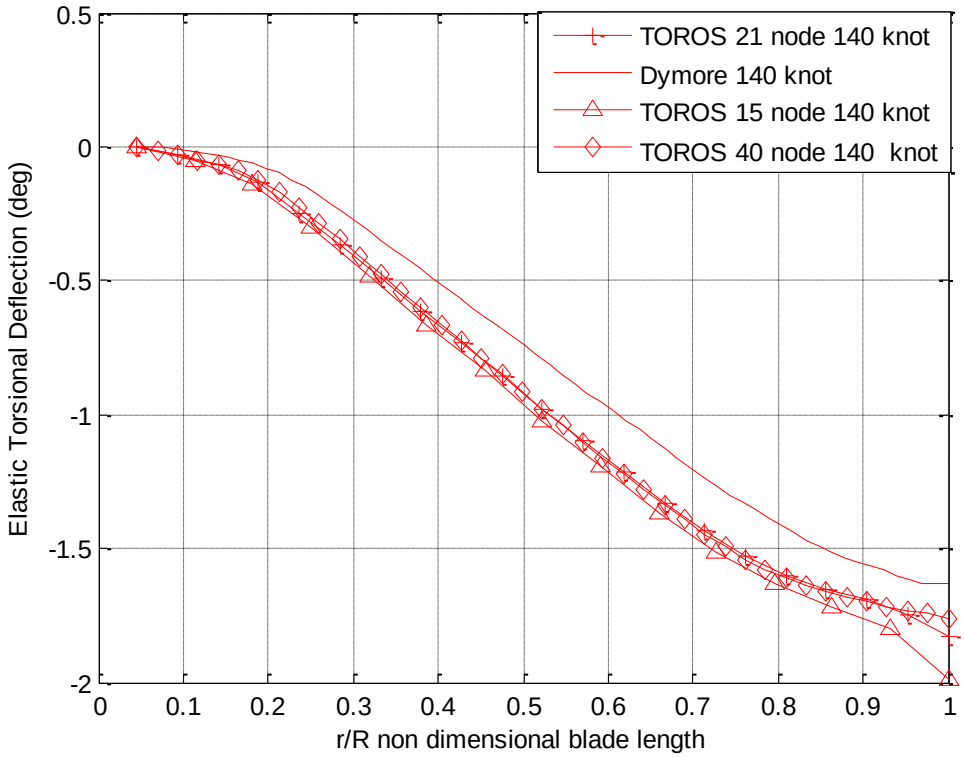

Figure 43 Comparison of TOROS 140 Knot Elastic Torsional Deflection Through Blade with Dymore

Figure 43 gives the 140 knot level flight elastic tip deflection comparison results of Dymore and Toros. At 140 knot, the twist predicted by Dymore is -1.63 degree, whereas twist predicted by Toros at 140 knot forward flight is -1.76 degree for the 40 node solution, -1.85 degree for the 21 node solution and -2 degree for the 15 node solution. The TOROS results are close with different node numbers up to 0.9R. However the 40 node result is smoother because of the tip deflection and the behavior of the deflection curve is similar to Dymore. This tip deflection gets better in terms of behavior as the FE node number in TOROS increases. The alternative way of getting better results in TOROS may be increasing the number of nodes close to tip, so taking coarse nodes up to tip and more dense nodes at the tip. In this work the finite element lengths are taken equal but variable length finite element modelling can be another solution of improving TOROS tip deflection results and comparison with Dymore. It is important to note that the difference between TOROS and Dymore results in terms of magnitude is less in hover than the 140 knot. At 140 knot the difference between Dymore and TOROS reaches up to 0.4 degree.

These differences are allowed due to the difference between trim algorithms of programs. At the same time Dymore is a structural analyses tool which includes improved elastic blade model but a simple trim algorithm, whereas in TOROS blade model is very simple but there is a powerful trim algorithm. However, it is considered that the results are satisfactory to verify the elastic blade modeling method implemented in TOROS.

CHAPTER 4

IMPLEMENTATION OF THE AEROELASTIC BEAM BLADE MODEL INTO FLIGHT DYNAMICS

Aeroelastic beam model is implemented to the Matlab/Simulink [20] environment and various flight dynamics simulations of the helicopter with the rigid and elastic blade are performed to study the effect of blade elasticity on the response of the helicopter. Analyses are done starting from simpler cases to more complicated flight conditions and maneuvers. First step is the wind tunnel trim, which means that the main rotor is trimmed, and roots of the trimmed system are analyzed. Then full helicopter trim is done in hover and in several forward flight velocities. After this step longitudinal static stability simulation tests are conducted. At the last step, transient analyses are done for maneuver simulation and an input is given after the helicopter is trimmed and behavior of the helicopter is observed.

The flight conditions simulated to observe the effect of blade elasticity are chosen according to the following criteria. Forward flight sweep is chosen since it includes velocities from hover to 150 knot forward flight trim so it is easier to see the trend of control inputs and Euler angles with flight speed. Autorotation is chosen because of the lower collective trim values required. Longitudinal stability tests are chosen in order to observe effect of blade elasticity on the stability of the helicopter. Finally certain transient analyses are conducted so as to observe that the effect of blade elasticity on the helicopter response in transient maneuvers.

In terms of helicopter flight mechanics important parameters are the control angles given by the pilot and the autopilot to control the helicopter, attitude of the helicopter, power required and supplied, main hub forces and moments and the flapping angles,

in other words the flapping of all individual blades and the final position of tip path plane. Generally all these parameters are checked for specific trim and maneuvers. The blade elasticity is expected to affect mostly the control angles and since the blade elastic is in the torsional direction, hence most of the effect is expected to be in the collective channel. The control angles are important because the limits of these controls are specified by flight mechanics group in design period.

4.1 Trim Analysis

Trim is done to find the equilibrium point of the helicopter in a certain time step under certain conditions. Trimming the helicopter neutralizes the forces required to keep the control surfaces in a position. In a trimmed helicopter there is force balance, hence the system flies at constant speed or rate.

In in house simulation tool, trim states and outputs are set as float and these are the parameters that can be perturbed to reach the target, inputs and state derivatives are set as freeze by default, the targets set to be reached. Using the initial states and inputs, system is run for one time step and new state derivatives and outputs are obtained. For the solution to be successful, free states and inputs must be equal to the constraints, target state derivatives and outputs. During the iteration, new state derivatives and outputs are evaluated in each step and error norm is calculated after each iteration step, and if the error norm is smaller than the trim tolerance value, the system is assumed to be successfully trimmed. In elastic the blade trim, the acceleration and velocity of the elastic torsion angle is zero, hence system solution becomes a static solution as defined in Section 3.1 in Eqn. (14) and Eqn.(15).

In trim analysis total flight speed, flight path angle, altitude, pressure, landing gear configuration, take off weight are given as input to the trim code. Freezed and floated variables can be also set in the trim command.

The implementation is done step by step to have accurate and reliable and trim analysis. First step is the wind tunnel trim tests. In wind tunnel trim, there is only main rotor dynamics and the system is trimmed to certain values such as no pitch and roll

CHAPTER 5

CONCLUSION

In order to estimate the rotor behavior more accurately, it is essential to have more accurate model in terms of rotor dynamics. In recent years there is an interest in increasing the fidelity of flight mechanics models. In the literature, there are two common points which people work on to generate higher fidelity flight mechanics models. One of them is the inflow model and the other one is taking the blade elasticity into account in rotor dynamics and eventually in the flight mechanics model of the full rotorcraft. Higher fidelity inflow and blade models together affect the modeling and results in a more realistic representation of rotor dynamics.

In this thesis, a methodology that includes elastic blade modeling in the torsional direction for flight dynamics applications is presented. This is a fast method specifically implemented to a flight mechanics model of a helicopter, and various trim and maneuver analyses are performed. In the implementation, blade is divided into sections and this section number is variable and depends on the user. For each section the equation of motion in torsional direction is solved utilizing the mass, torsional stiffness of the blade sections. Then mass and stiffness matrices are formed and equation is solved for torsional deformation along the span of the blade.

It is concluded that the effect of flexibility in the torsional direction changes the pitch angle of the blade, and the torsionally elastic blade has a lower pitch angle and hence for the same trim condition elastic blade needs a higher collective input than the rigid blade to satisfy the same trim condition. Since the results show that the direct effect of elastic blade model in the torsional direction, is in the collective channel, the mean shaft force and moments are expected to be similar for a trim condition. It is aldo seen that the torsional elasticity does not have a significant effect on the lateral and the

longitudinal collective controls. The attitude of the helicopter, the power required and flapping angles are also similar for both rigid and elastic blade conditions.

For this particular study and results show that modeling the blade torsional flexibility has an effect on collective input and this effect increases with velocity. At 140 knot level flight the increase in collective is 1.68 degree. Lateral and longitudinal cyclic inputs do not change in hover with the modeling of flexibility whereas at 140 knot there is a slight change comes with the elastic blade modelling.

For autorotation significant change again is in the collective channel which is around 1 degree regardless of the indicated airspeed.

For stability the results clearly show that elastic blade modeling has a negative effect on the longitudinal stability of the helicopter. In the autorotation case, static stability results are almost unstable which is not observed in the rigid blade modeling. In other cases like cruise, climb and flight at V_{Ne} speed elastic blade makes the stability worse but the results are still stable, in other words the slope of the longitudinal input versus airspeed curve is still negative.

To sum up elastic blade can result in a 1 to 1.8 degree change in collective angle depending on the flight condition. The range of change for longitudinal and lateral inputs varies according to the flight condition but always less than 0.5 degree. Last but not least, the torsionally flexible blade model makes stability worse and even unstable for specific flight cases like autorotation.

In literature the main advantage of elastic blade modeling is stated as more accurate hub load prediction, more accurate off axis response and more accurate control input prediction.

In this study it is hard to comment on the accuracy of the off axis response and hub load prediction since there is no available flight test data of the current helicopter. In trim condition, pitch angle of the blade changes due to elasticity which results in a 1 to 2 degree increment in the collective angle. This affects the limits of control inputs set by flight mechanics group. Since predicting the right control input is important and one of the main aims of the flight mechanics group, elastic blade model becomes an

important part of modelling. At the trim conditions, hub loads and moments are not expected to differ with elastic blade model since system is trimmed to the same flight condition. Collective increases to compensate the difference in the pitch angle and to satisfy the same trim condition. However in transient cases, hub loads differ in the helicopter with the elastic blade to rigid blade since the same collective control is applied. With the control applied, elastic blade achieves a worse maneuver since the effective pilot input used to perform the maneuver is less due to the elastic blade pitch which reduces the effective angle of attack of the blade sections and decreases the maneuver performance. Although the differences are small, the effect is important to note.

Last but not least it is very important to consider that the results in this study is for a particular design which has a selected stiffness distribution, aerodynamic center, cg distribution, mass distribution, shear axis and feathering axis. For a different design the effect of torsional elasticity may be different in terms of magnitude and effect.

To conclude knowing the elastic effects and including these effects in a time efficient way in the flight mechanics simulations and models is beneficial and results in more accurate predictions of the real helicopter behavior.

As an intermediate future work, blade elasticity in the flapwise and edgewise directions can be implemented to achieve a fully elastic rotor blade model. It is deemed that the blade elasticity in the flapwise direction will be important just as the torsional elasticity. Also comparison of the hub loads predicted with the rigid and elastic blade models with the real experimental data would be very valuable in order to evaluate the effect of including blade elasticity in flight mechanics models of helicopters.

REFERENCES

[1] Howlett J.J., "UH-60A black Hawk Engineering Simulation Program," in *Volume II-Mathematical Model*, 1981.

[2] Zhao, X., and Curtiss, H. C.,, "A Linearized Model of Helicopter Dynamics Including Correlation with Flight Test," College Park, 1988.

[3] Miller, D. G., and White, F.,, "A Treatment of the Impact of Rotor Fuselage Coupling on Helicopter Handling Qualities," St. Louis, 1987.

[4] Padfield G. D., "On the Use of Approximate Models in Helicopter Flight Mechanics," *Vertica*, vol. 5, 1981.

[5] Brown, R. E., Housten S. S., «Comparison of Induced Velocity Models For Helicopter Flight Mechanics,» *Journal of Aircraft*, pp. 623-629, 2000.

[6] Lewis W. D., "An Aeroelastic Model Structure Investigation for a Manned Real Time Rotorcraft Simulation," in *American Helicopter Society 49th Annual Forum Proceedings*, St. Louis, 1993.

[7] Sturisky, S. H. Schrage D. P., "System Identification Validation of an AH-64 Aeroelastic Simulation Model," in *American Helicopter Society 49th Annual Forum Proceedings*, St. Louis, 1993.

[8] Turnour, S. R., Celi, R., "Modelling of Flexible Rotor Blades for Helicopter Flight Dynamics Applications," *Journal of the American Helicopter Society*, vol. 40, pp. 52-66, 1996.

[9] Kim F.D., Celi, R., Tischler, M. B.,, "Forward Flight Trim and Frequency Response Validation of a Helicopter Simulation Model," *Journal of Aircraft*, vol. 30, pp. 854-863, 1993.

[10] Spence, A. M., Celi, R.,, "Coupled Rotor-Fuselage Dynamics and Aeroelasticity in Turning Flight," *Journal of American Helicopter Society,* vol. 40, pp. 47-58, 1995.

[11] Peters, D. A., Boyd, D. D., He, C. J., "Finite State Induced Flow Model for Rotors in Hover and Forward Flight," *Journal of the American Helicopter Society,* vol. 34, pp. 5-17, 1989.

[12] Peters, D. A., He, C. J.,, "Correlation of Measured Induced Velocities with a Finite-State Wake Model," *Journal of American Helicopter Society,* vol. 36, pp. 59-70, 1991.

[13] Theodore C., "Helicopter Flight Dynamics Simulation with Refined Aerodynamic Modelling," University of Maryland, 2000.

[14] Piziali R. A., "Method for the Solution of the Aeroelastic Response Problem for Rotating Wings," *Journal of Sound and Vibration,* vol. IV, pp. 445-489, 1966.

[15] Johnson W., Rotorcraft Aeromechanics, Madrid: Cambridge University Press, 2013.

[16] AGARD, «Helicopter Weapon System Integration,» North Atlantic Treaty Organization, Winchester, 1997.

[17] ART, «Flightlab Theory Manual,» Advanced Rotorcraft Technology, Inc., California, 2008.

[18] Lienemann J., Greiner A., Rudnyi E. B., Korvink J. G., «Linear Beam Model,» IMTEK, Freiburg, 2004.

[19] Bauchau O., «Simulation Tools for Flexible Multibody Systems Users Manual,» University of Maryland, maryland.

[20] Mathworks, "The official Matlab software".

[21] Balmford D.,Bramwell A.R.S., Done G., Bramwells Helicopter Dynamics, Butterworth Heinemann, 2001.